30. Prefontaine D, Lajoie-Kadoch S, Foley S, Audusseau S, Olivenstein R, et al. (2009) Increased expression of IL-33 in severe asthma: evidence of expression by airway smooth muscle cells. J Immunol 183: 5094–5103.
31. Matsuda A, Okayama Y, Terai N, Yokoi N, Ebihara N, et al. (2009) The role of interleukin-33 in chronic allergic conjunctivitis. Invest Ophthalmol Vis Sci 50: 4646–4652.
32. Pushparaj PN, Tay HK, H'Ng SC, Pitman N, Xu D, et al. (2009) The cytokine interleukin-33 mediates anaphylactic shock. Proc Natl Acad Sci U S A 106: 9773–9778.
33. Hoshino K, Kashiwamura S, Kuribayashi K, Kodama T, Tsujimura T, et al. (1999) The absence of interleukin 1 receptor-related T1/ST2 does not affect T helper cell type 2 development and its effector function. J Exp Med 190: 1541–1548.
34. Mangan NE, Dasvarma A, McKenzie AN, Fallon PG (2007) T1/ST2 expression on Th2 cells negatively regulates allergic pulmonary inflammation. Eur J Immunol 37: 1302–1312.
35. Kurowska-Stolarska M, Kewin P, Murphy G, Russo RC, Stolarski B, et al. (2008) IL-33 induces antigen-specific IL-5$^+$ T cells and promotes allergic-induced airway inflammation independent of IL-4. J Immunol 181: 4780–4790.
36. Meisel C, Bonhagen K, Lohning M, Coyle AJ, Gutierrez-Ramos JC, et al. (2001) Regulation and function of T1/ST2 expression on CD4$^+$ T cells: induction of type 2 cytokine production by T1/ST2 cross-linking. J Immunol 166: 3143–3150.
37. Kearley J, Buckland KF, Mathie SA, Lloyd CM (2009) Resolution of allergic inflammation and airway hyperreactivity is dependent upon disruption of the T1/ST2-IL-33 pathway. Am J Respir Crit Care Med 179: 772–781.
38. Coyle AJ, Lloyd C, Tian J, Nguyen T, Erikkson C, et al. (1999) Crucial role of the interleukin 1 receptor family member T1/ST2 in T helper cell type 2-mediated lung mucosal immune responses. J Exp Med 190: 895–902.
39. Oshikawa K, Yanagisawa K, Tominaga S, Sugiyama Y (2002) Expression and function of the ST2 gene in a murine model of allergic airway inflammation. Clin Exp Allergy 32: 1520–1526.
40. Lohning M, Stroehmann A, Coyle AJ, Grogan JL, Lin S, et al. (1998) T1/ST2 is preferentially expressed on murine Th2 cells, independent of interleukin 4, interleukin 5, and interleukin 10, and important for Th2 effector function. Proc Natl Acad Sci U S A 95: 6930–6935.
41. Culley FJ (2009) Natural killer cells in infection and inflammation of the lung. Immunology 128: 151–163.
42. Umetsu DT, DeKruyff RH (2006) A role for natural killer T cells in asthma. Nat Rev Immunol 6: 953–958.
43. Espinassous Q, Garcia-de-Paco E, Garcia-Verdugo I, Synguelakis M, von Aulock S, et al. (2009) IL-33 enhances lipopolysaccharide-induced inflammatory cytokine production from mouse macrophages by regulating lipopolysaccharide receptor complex. J Immunol 183: 1446–1455.
44. Ohno T, Oboki K, Kajiwara N, Morii E, Aozasa K, et al. (2009) Caspase-1, caspase-8, and calpain are dispensable for IL-33 release by macrophages. J Immunol 183: 7890–7897.
45. Hoshino K, Takeuchi O, Kawai T, Sanjo H, Ogawa T, et al. (1999) Cutting edge: Toll-like receptor 4 (TLR4)-deficient mice are hyporesponsive to lipopolysaccharide: evidence for TLR4 as the Lps gene product. J Immunol 162: 3749–3752.
46. Townsend MJ, Fallon PG, Matthews DJ, Jolin HE, McKenzie AN (2000) T1/ST2-deficient mice demonstrate the importance of T1/ST2 in developing primary T helper cell type 2 responses. J Exp Med 191: 1069–1076.
47. Naito A, Azuma S, Tanaka S, Miyazaki T, Takaki S, et al. (1999) Severe osteopetrosis, defective interleukin-1 signalling and lymph node organogenesis in TRAF6-deficient mice. Genes Cells 4: 353–362.
48. Oboki K, TOhno, NKajiwara, KArae K, HMorita, et al. (2010) IL-33 is a crucial amplifier of innate rather than acquired immunity. Proc Natl Acad Sci U S A 107: 18581–18586.
49. Moritz DR, Gheyselinck J, Klemenz R (1998) Expression analysis of the soluble and membrane-associated forms of the interleukin-1 receptor-related T1 protein in primary mast cells and fibroblasts. Hybridoma 17: 107–116.
50. Moritz DR, Rodewald HR, Gheyselinck J, Klemenz R (1998) The IL-1 receptor-related T1 antigen is expressed on immature and mature mast cells and on fetal blood mast cell progenitors. J Immunol 161: 4866–4874.
51. Walzl G, Matthews S, Kendall S, Gutierrez-Ramos JC, Coyle AJ, et al. (2001) Inhibition of T1/ST2 during respiratory syncytial virus infection prevents T helper cell type 2 (Th2)- but not Th1-driven immunopathology. J Exp Med 193: 785–792.
52. Xu D, Chan WL, Leung BP, Huang F, Wheeler R, et al. (1998) Selective expression of a stable cell surface molecule on type 2 but not type 1 helper T cells. J Exp Med 187: 787–794.
53. Luthi AU, Cullen SP, McNeela EA, Duriez PJ, Afonina IS, et al. (2009) Suppression of interleukin-33 bioactivity through proteolysis by apoptotic caspases. Immunity 31: 84–98.
54. Cayrol C, Girard JP (2009) The IL-1-like cytokine IL-33 is inactivated after maturation by caspase-1. Proc Natl Acad Sci U S A 106: 9021–9026.
55. Kawakami T, Kitaura J, Xiao W, Kawakami Y (2005) IgE regulation of mast cell survival and function. Novartis Found Symp 271: 100–107. discussion 108–114, 145–151.
56. Xu D, Jiang HR, Kewin P, Li Y, Mu R, et al. (2008) IL-33 exacerbates antigen-induced arthritis by activating mast cells. Proc Natl Acad Sci U S A 105: 10913–10918.
57. Leung BP, Xu D, Culshaw S, McInnes IB, Liew FY (2004) A novel therapy of murine collagen-induced arthritis with soluble T1/ST2. J Immunol 173: 145–150.
58. Palmer G, Talabot-Ayer D, Lamacchia C, Toy D, Seemayer CA, et al. (2009) Inhibition of interleukin-33 signaling attenuates the severity of experimental arthritis. Arthritis Rheum 60: 738–749.
59. McGuirk P, McCann C, Mills KH (2002) Pathogen-specific T regulatory 1 cells induced in the respiratory tract by a bacterial molecule that stimulates interleukin 10 production by dendritic cells: a novel strategy for evasion of protective T helper type 1 responses by Bordetella pertussis. J Exp Med 195: 221–231.
60. Dinarello CA (2009) Immunological and inflammatory functions of the interleukin-1 family. Annu Rev Immunol 27: 519–550.
61. Sims JE, Smith DE (2010) The IL-1 family: regulators of immunity. Nat Rev Immunol 10: 89–102.
62. Gutcher I, Urich E, Wolter K, Prinz M, Becher B (2006) Interleukin 18-independent engagement of interleukin 18 receptor-α is required for autoimmune inflammation. Nat Immunol 7: 946–953.
63. Pan G, Risser P, Mao W, Baldwin DT, Zhong AW, et al. (2001) IL-1H, an interleukin 1-related protein that binds IL-18 receptor/IL-1Rrp. Cytokine 13: 1–7.
64. Lin H, Ho AS, Haley-Vicente D, Zhang J, Bernal-Fussell J, et al. (2001) Cloning and characterization of IL-1HY2, a novel interleukin-1 family member. J Biol Chem 276: 20597–20602.
65. Bulek K, Swaidani S, Qin J, Lu Y, Gulen MF, et al. (2009) The essential role of single Ig IL-1 receptor-related molecule/Toll IL-1R8 in regulation of Th2 immune response. J Immunol 182: 2601–2609.
66. Drube S, Heink S, Walter S, Lohn T, Grusser M, et al. (2010) The receptor tyrosine kinase c-Kit controls IL-33 receptor signaling in mast cells. Blood 115: 3899–3906.
67. Baekkevold ES, Roussigne M, Yamanaka T, Johansen FE, Jahnsen FL, et al. (2003) Molecular characterization of NF-HEV, a nuclear factor preferentially expressed in human high endothelial venules. Am J Pathol 163: 69–79.
68. Carriere V, Roussel L, Ortega N, Lacorre DA, Americh L, et al. (2007) IL-33, the IL-1-like cytokine ligand for ST2 receptor, is a chromatin-associated nuclear factor in vivo. Proc Natl Acad Sci U S A 104: 282–287.
69. Roussel L, Erard M, Cayrol C, Girard JP (2008) Molecular mimicry between IL-33 and KSHV for attachment to chromatin through the H2A-H2B acidic pocket. EMBO Rep 9: 1006–1012.

Molecular Human Reproduction, Vol.17, No.7 pp. 447–452, 2011
Advanced Access publication on February 2, 2011 doi:10.1093/molehr/gar008

MHR ORIGINAL RESEARCH

Polymorphisms in the annexin A5 gene promoter in Japanese women with recurrent pregnancy loss

Hironori Miyamura[1,2], Haruki Nishizawa[2], Sayuri Ota[1], Machiko Suzuki[1], Ayaka Inagaki[1,2], Hiromi Egusa[1,2], Sachie Nishiyama[1,2], Takema Kato[1], Kanako Pryor-Koishi[2], Isao Nakanishi[3], Tomio Fujita[3], Yuzo Imayoshi[3], Arseni Markoff[4], Itaru Yanagihara[3], Yasuhiro Udagawa[2], and Hiroki Kurahashi[1,*]

[1]Division of Molecular Genetics, Institute for Comprehensive Medical Science, Fujita Health University, 1-98 Dengakugakubo, Kutsukake-cho, Toyoake, Aichi 470-1192, Japan [2]Department of Obstetrics and Gynecology, Fujita Health University School of Medicine, Toyoake, Aichi 470-1192, Japan [3]Osaka Medical Center and Research Institute for Maternal and Child Health, Izumi, Osaka 594-1101, Japan [4]Institute of Medical Biochemistry, Center for Molecular Biology of Inflammation, University of Muenster, D-48149 Muenster, Germany

*Correspondence address. Tel: +81-562-93-9391; Fax: +81-562-93-8831; E-mail: kura@fujita-hu.ac.jp

Submitted on September 16, 2010; resubmitted on January 21, 2011; accepted on January 25, 2011

ABSTRACT: Recent findings have raised the possibility that polymorphisms within the annexin A5 gene (*ANXA5*) promoter contribute to the etiology of recurrent pregnancy loss (RPL). In our present study, 243 Japanese women who had suffered more than three fetal losses and a group of 119 fertile controls were genotyped for four *ANXA5* gene promoter single-nucleotide polymorphisms (SNPs; SNP1-4: g.-467G>A, g.-448A>C, g.-422T>C, g.-373G>A) previously reported to be associated with this disorder. An additional two SNPs located within the 5′-untranslated region of the *ANXA5* (SNP5 and 6: g.-302T>G, g.-1C>T) were also evaluated. Our case–control study revealed that the minor allele was significantly more frequent in the RPL group than controls for all six of these SNPs, among which SNP5 showed the highest significance ($P = 0.002$). As with the M2 haplotype for SNP1-4 (A-C-C-A) for a western population in previous reports, a haplotype comprising all of the minor alleles for SNP1-6 (A-C-C-A-G-T), the third major haplotype in the Japanese population, showed a significantly higher frequency in our current RPL subjects than in controls ($P = 0.025$). In addition, the second major haplotype (G-A-T-G-G-C) was found to confer a significant risk of RPL ($P = 0.036$), implicating SNP5 as a major risk determinant for this disease. Our present findings support the hypothesis that genomic variations within the *ANXA5* gene upstream region impact upon the disease susceptibility to RPL. Our data indicate that SNP5 is a novel risk factor for this disease in the Japanese population.

Key words: recurrent pregnancy loss / annexin A5 / promoter / SNP / haplotype

Introduction

Recurrent pregnancy loss (RPL) is a serious reproductive problem affecting ~5% of couples trying to conceive (Sierra and Stephenson, 2006). This disorder is caused by many etiologies, including structural, infective, endocrine, immune and coagulation disorders (Rai and Regan, 2006). However, most of the cases are of an unexplained cause, and this has hindered the development of therapeutic interventions for this serious condition. Couples have thus been treated only empirically, based on anecdotal evidence (Rai and Regan, 2006).

To date, a considerable body of evidence has indicated that genetic factors significantly contribute to the etiology of RPL (Ward, 2000; Sierra and Stephenson, 2006). It is thus possible that RPL develops as a single gene disorder. We recently reported that two women with RPL had a heterozygous mutation within the meiosis-expressing gene, *SYCP3*, indicating that a small subset of cases is caused by a recurrent chromosomal segregation error during meiotic division in the oocytes (Bolor *et al.*, 2009). However, another prevailing hypothesis is that most instances of RPL are due to a polygenic disorder and are associated with multiple gene mutations (Coulam *et al.*, 2006).

Annexin A5 (*ANXA5*) is both a Ca^{2+} and phospholipid-binding protein that is localized at the surface of the placental syncytiotrophoblast layer and performs a vital anticoagulant function in the maternal blood at the intervillous space (Gerke and Moss, 2002). It has recently

been shown that polymorphisms in the promoter region of the *ANXA5* gene are significantly associated with RPL, and that women with an M2 haplotype have more than a 2-fold higher risk of fetal loss than non-carriers (Bogdanova *et al.*, 2007). In our present study, we further examined upstream *ANXA5* gene variants among a cohort of Japanese RPL cases.

Materials and Methods

Patients

A total of 243 Japanese women with a history of RPL (more than three consecutive pregnancy losses) of unknown cause were recruited from Fujita Health University Hospital and the Osaka Medical Center and Research Institute for Maternal and Child Health (aged 34.15 ± 4.27 years; gravidity, 3.14 ± 0.51; parity, 0.083 ± 0.319; fetal losses, 3.06 ± 0.30). None of these individuals had any family history of birth defects. RPL cases of known cause such as hormonal, structural, immunological and coagulation disorders were excluded. All of these women were examined by ultrasonography or hysterosalpingography to detect any possible anatomic abnormalities of the genital tract, and had blood drawn to examine for immunologic risk factors, including anti-nuclear antibodies, and anti-phospholipid antibodies such as lupus anticoagulant. Cases with either inherited or acquired thrombophilia, as determined by measurements of the plasma levels of antithrombin III, and proteins C and S, were excluded. Screening for the Leiden mutation (1691G>A) within the *F5* gene and the PTm mutation (20210G>A) of the *F2* gene was performed using the Taqman assay (rs6025 and rs1799963, respectively) but no positive cases were found. Blood tests for hyperthyroidism, diabetes mellitus, hyperprolactinemia and infections such as chlamydia were also performed. Cytogenetic analyses demonstrated a normal karyotype in all of these individuals as well as in their partners, but were not performed in all of the abortuses. Peripheral blood samples were obtained at the clinic after appropriate informed consent was obtained. A total of 119 blood samples from Japanese women with at least one child and no history of infertility or miscarriage were used as controls (age at sampling, 46 ± 13.5 years). This study was approved by the Ethical Review Board for Human Genome Studies at Fujita Health University (Accession numbers 39 and 82, approved on 4 October 2004 and 22 May 2009, respectively), and at Osaka Medical Center and Research Institute for Maternal and Child Health (Accession number 214-2, approved on 12 February 2010).

Isolation of genomic DNA and analyses of variants

Genomic DNA was extracted from peripheral blood samples using PureGene (Gentra Systems, Minneapolis, MN). The primers used to amplify the promoter region of the human *ANXA5* gene (GenBank Accession Number: AC096730) were as follows: Fw, CCGAGCCCTGGACA GCTCCCCA; Rv, AGAGGAGAGCGTGGTCGCGGGGC (Bogdanova *et al.*, 2007). PCR was performed for 45 cycles of 10 s at 98°C and 5 min at 68°C. After the removal of PCR primers and excess dNTPs by exonuclease I and shrimp alkaline phosphatase (ExoSAP-IT, USB Corp., Cleveland, OH), the amplified products were directly sequenced using the primers and the ABI Prism Sequencer 3130XL (Applied Biosystems, Foster City, CA). Taqman primers and probes were purchased to genotype the −1C>T single-nucleotide polymorphism (SNP) of the *ANXA5* gene (rs11575945) in accordance with the manufacturer's protocol (Applied Biosystems).

Statistical analysis

Deviations from a Hardy–Weinberg equilibrium (HWE) among the genotypes were first evaluated using the χ^2 test. Genotype and allele frequency differences between the RPL and control groups were then evaluated by $\chi 2$ analysis. Linkage disequilibrium (LD) was evaluated for all SNPs as were the Lewontin's D' (|D'|) and the LD coefficient r^2 between all pairs of biallelic loci. We estimated the haplotype frequencies among the RPL and control groups using the maximum-likelihood method employing an expectation-maximization algorithm. Haplotype-wise association analysis was evaluated using a likelihood ratio test. All statistical analyses were performed by univariate analyses. In addition, multivariate logistic analysis was also performed for the determination of epistasis. All of these calculations were performed using SNPAlyze software (Dynacom, Chiba, Japan).

Results

We sequenced the promoter region of the *ANXA5* gene in 243 Japanese women with RPL and 119 fertile controls and thereby identified four variations that had been previously reported by Bogdanova *et al.* (2007), i.e. SNP1 (g.-467G>A) and SNP2 (g.-448A>C, rs28717001) in the untranscribed promoter region, and SNP3 (g.-422T>C, rs28651243) and SNP4 (g.-373G>A) within the 5′ untranslated exon (exon 1; Fig. 1). SNP5 (g.-302T>G, rs1050606) is another

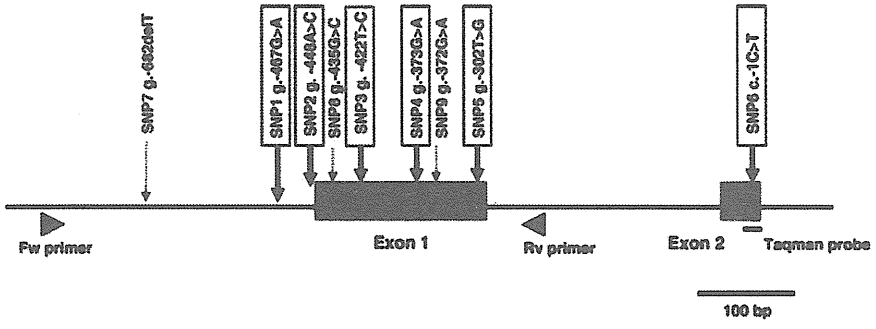

Figure 1 *ANXA5* gene promoter variants. Exons are indicated by boxes and the coding region is denoted by a black box. Vertical arrows indicate the location of six common SNPs (thick arrows) and three rare SNPs (thin arrows). Triangles indicate the position recognized by primers used to amplify the promoter region. The horizontal short bar indicates the regions associated with the Taqman primers and probe.

common polymorphism located within exon 1. We performed further genotyping for another common *ANXA5* SNP, g.-1C>T (SNP6, rs11538099), which is located one nucleotide upstream of the initiation codon in exon 2. The genotype frequencies for all of the six SNPs examined were found to be in HWE, suggesting neither sampling bias nor mistyping of genotypes (Table I). In addition, we identified three rare SNPs that have not been previously reported. A single nucleotide deletion was identified upstream of SNP1 (SNP7, g.-682delT) but this variation was found in only one RPL case as a heterozygote. A further SNP (SNP8, g.-435G>C) was identified between SNP2 and SNP3 in two RPL subjects and one control also as a heterozygote. The third rare variant was found at one nucleotide downstream of SNP4 within exon 1 (SNP9: g.-372G>A) in a control subject as a heterozygote. These rare variants were excluded from further study on the basis of the common disease–common variant hypothesis.

We performed a case-control study for the six common *ANXA5* SNPs in the RPL and fertile control groups. The carrier frequency for the minor alleles was found to be significantly higher in the RPL group for all six SNPs ($P < 0.05$) in both allele-wise and genotype-wise (dominant model) analyses (Table II). Our statistical analyses further indicated that the most significant difference between the groups was for SNP5 (genotype-wise: $P = 0.007$, allele-wise: $P = 0.002$). Women carrying this minor allele were found to have about a 2-fold higher risk of fetal loss than non-carriers. However, SNP4 conferred the highest risk of RPL [odds ratio (OR) = 2.369 Table II]. Since the minor allele frequency was relatively high for SNP5, we also performed recessive model analysis for this polymorphism. Homozygotes of the SNP5 minor allele were more frequent in the RPL group ($P = 0.02$), and this genotype conferred a 7-fold higher risk of RPL (OR = 7.76).

We next performed LD analysis among the six *ANXA5* SNPs (Fig. 2). All except for SNP5 manifested a strong LD as was previously reported for SNP1–4 (Bogdanova *et al.*, 2007). We further performed haplotype-wise analysis for these six SNPs, which indicated the presence of three major haplotypes in a Japanese population (Table III). G-A-T-G-T-C and G-A-T-G-G-C were the two major haplotypes and accounted for >90% of the subjects. The first four (G-A-T-G)

Table I Case–control study of the six common *ANXA5* promoter SNPs.

	Alleles	SNP ID	Phenotype	N[a]	HWE[b]	MAF[c]	Genotype deviation		
							M/M	M/m	m/m
SNP1	−467G >A	N.A.	Cases	243	0.389	0.107	192	50	1
			Controls	119	0.884	0.059	106	12	1
SNP2	−448A>C	rs28717001	Cases	243	0.330	0.111	190	52	1
			Controls	119	0.966	0.063	105	13	1
SNP3	−442T>C	rs28651243	Cases	243	0.330	0.111	190	52	1
			Controls	119	0.966	0.063	105	13	1
SNP4	−373G>A	N.A.	Cases	243	0.389	0.107	192	50	1
			Controls	119	0.797	0.055	107	11	1
SNP5	−302T>G	rs1050606	Cases	243	0.506	0.228	147	81	15
			Controls	119	0.675	0.130[d]	89	29	1
SNP6	−1C>T	rs11575945	Cases	243	0.421	0.105	193	49	1
			Controls	119	0.838	0.059	106	12	1

[a]Number.
[b]Hardy–Weinberg equilibrium.
[c]Minor allele frequency.
[d]0.150 is reported for general Japanese population in the HapMap database.

Table II Association between *ANXA5* SNPs and RPL.

	Dominant model			Allele model		
	P-value	OR[a]	95% CI[b]	*P*-value	OR[a]	95% CI[b]
SNP1	0.018	2.166	1.127–4.163	0.034	1.917	1.040–3.535
SNP2	0.021	2.092	1.108–3.949	0.039	1.858	1.026–3.367
SNP3	0.021	2.092	1.108–3.949	0.039	1.858	1.026–3.367
SNP4	0.010	2.369	1.210–4.637	0.021	2.074	1.106–3.889
SNP5	0.007	1.937	1.190–3.154	0.002	1.977	1.282–3.047
SNP6	0.023	2.112	1.098–4.065	0.042	1.876	1.016–3.463

[a]Odds ratio.
[b]Confidence interval (low–high).

	SNP1	SNP2	SNP3	SNP4	SNP5	SNP6
SNP1		1	1	1	1	1
SNP2	0.929		1	1	1	1
SNP3	0.929	1.000		1	1	1
SNP4	0.924	0.859	0.859		1	1
SNP5	0.417	0.449	0.449	0.386		1
SNP6	1.000	0.929	0.929	0.924	0.417	

Figure 2 LD analyses of the six common *ANXA5* gene promoter SNPs. Lewontin's D' (|D'|) scores between all SNP pairs are indicated at the upper right. The LD coefficients r^2 values are shown at the lower left. The dark grey areas indicate a strong LD with high r^2 values.

Table III Association of *ANXA5* SNP haplotypes with RPL.

	Cases	Controls	χ^2	*P*-value	OR[a]	95% CI[b]
SNP1–6[c]						
G-A-T-G-T-C	0.772	0.870	9.766	0.002	0.506	0.328–0.780
G-A-T-G-G-C	0.117	0.067	4.423	0.036	1.844	1.035–3.285
A-C-C-A-G-T	0.105	0.055	5.017	0.025	2.029	1.081–3.810
SNP1–4[c]						
G-A-T-G	0.889	0.937	4.289	0.038	0.538	0.297–0.975
A-C-C-A	0.107	0.055	5.368	0.021	2.074	1.106–3.889

[a]Odds ratio.
[b]Confidence interval (low–high).
[c]Only haplotypes with a frequency >1.0% are listed.

SNPs constitute the *N* haplotype described previously by Bogdanova *et al.* (2007). The haplotype comprising all six minor alleles (A-C-C-A-G-T) was found to be the third most common. The first four SNPs (A-C-C-A) constitute the so-called M2 haplotype, the frequency of which is 5.4% in the general Japanese population. This is lower than the rate reported for western countries (~16%). The M1 haplotype (G-C-C-G) was found to be rare in Japanese subjects (data not shown). We subsequently performed a case-control study for these haplotypes, and found that A-C-C-A-G-T was significantly more frequent in RPL samples (10.5 versus 5.5%, $P = 0.025$). This haplotype also appeared to pose a 2.35-fold higher risk of RPL compared with non-carriers. This is consistent with the previous finding that the M2 haplotype is more frequent in RPL samples (10.7 versus 5.5%, $P = 0.021$).

It was of interest that the G-A-T-G-G-C haplotype, which comprises all major alleles except SNP5, was also found to be more frequent in RPL samples (11.7 versus 6.7%, $P = 0.036$) (Table III). This haplotype appeared to pose a 1.84-fold higher risk of RPL than non-carriers. The fact that not only the A-C-C-A-G-T haplotype that includes M2, but also the G-A-T-G-G-C haplotype was found to be more frequent in the RPL group suggests that SNP5 is a major risk determinant for this disorder. Since SNP5 and the other five SNPs are in weak LD, SNP5 and M2 haplotype may have confounding effects. However, based on the results of our logistic regression analysis, it is not certain whether SNP5 is epistatic to the M2 haplotype ($P = 0.086$ for SNP5 versus $P = 0.292$ for M2). Taken together, however, and regardless of whether it is independent of or dependent on the M2 haplotype, the minor allele of SNP5 may potentially contribute to the etiology of RPL in the Japanese population.

Discussion

The M2 haplotype of the *ANXA5* gene promoter was recently reported to associate with RPL in a population of 70 women with more than two fetal losses (18 in 70 RPL cases versus 41 in 500 controls) (Bogdanova *et al.*, 2007). In another study of larger cohorts, the M2 haplotype was recorded in 35 of 103 women with RPL and in 30 of 154 controls, and the frequency was reported to be significantly higher in the RPL group ($P < 0.001$) (Tiscia *et al.*, 2009). In our current study, we found that the A-C-C-A-G-T haplotype of the *ANXA5* gene promoter is associated with RPL in a Japanese population, which is consistent with previous data reported for western populations. Each of the variants tested in our analysis was found to be located within the upstream regulatory region of the

ANXA5 gene. Reporter assays have previously indicated that the transcription efficiency from susceptible *ANXA5* variants is lower than that in the major variants (Bogdanova *et al.*, 2007). This suggests that these SNPs are functional and can decrease the expression of *ANXA5*, thereby impacting upon the etiology of RPL.

We further found that among the polymorphisms tested in our current analysis, SNP5 (g.-302T>G) is also associated with RPL. Our LD analyses indicated that this SNP is not tightly linked to the M2 haplotype and our results raise the possibility that it may be the primary determinant of the risk of RPL in Japanese women. Since SNP5 was not analyzed in previous reports, we are unsure at present whether this polymorphism is also associated with RPL in western cohorts. Whereas the National Center for Biotechnology Information database reports an allele frequency of 15/85 for G/T in the Japanese population, this rises to as high as 54/46 for western populations (Centre d'Etudes du Polymorphisme Humaine). On the other hand, the frequency of the M2 haplotype is 5.5% in the Japanese population, but 16% in western cohorts, which is similar to the rate of the g.-302T>G SNP in Japan. A more thorough analysis using different cohorts of RPL cases would reinforce our conclusion that the SNP5 might be the primary risk determinant.

The *ANXA5* protein is localized at the apical surfaces of the syncytiotrophoblast layer in chorionic villi (Krikun *et al.*, 1994). Interestingly, the infusion of anti-*ANXA5* antibodies induces coagulation at the surfaces of the syncytiotrophoblast layer, leading to fetal loss, which indicates that *ANXA5* protects the feto–maternal interface from the coagulation of maternal blood (Wang *et al.*, 1999). Further, experimental data have indicated that anti-phospholipid antibodies facilitate coagulation by reducing the levels of *ANXA5* at the surface of the trophoblasts in antiphospholipid syndrome (APS), a well-established condition that manifests as RPL (Rand *et al.*, 1997; Shapiro, 1996). Transcription of the *ANXA5* gene from the M2 haplotype appears to be at a lower level than the standard haplotype (Bogdanova *et al.*, 2007). It is thus reasonable to speculate that women carrying the M2 haplotype, and possibly the minor allele of SNP5, have low levels of ANXA5 protein at the surfaces of their trophoblasts. This will induce a greater susceptibility to coagulation and thus RPL. In this context, RPL in women with the M2 haplotype and APS may belong to the same clinical entity, annexinopathy (Rand, 2000). Indeed, frequent M2 haplotype has been reported in other obstetric complications such as pre-eclampsia and pregnancy-related venous thromboembolism, which may also belong to annexinopathy (Tiscia *et al.*, 2009; Grandone *et al.*, 2010a, b).

We genotyped DNA from maternal leukocytes in our current analysis, as has been done previously (Bogdanova *et al.*, 2007; Tiscia *et al.*, 2009). It was also reported earlier that the placental expression of ANXA5 at the mRNA level is related to the maternal genotype (Chinni *et al.*, 2009). This is an intriguing finding since the syncytiotrophoblasts that carry ANXA5 protein at their surface are of fetal origin and have a half-maternal and half-paternal genome. Although the *ANXA5* gene is expressed abundantly in the placenta, somewhat low level of expression is observed ubiquitously. It is not yet certain whether ANXA5 protein at the syncytiotrophoblast surfaces originates from the maternal circulation or is produced by the fetal syncytiotrophoblasts. Further investigations, including the genotyping of the fetus or placenta from RPL cases, will be necessary to elucidate this phenomenon.

Although a recent study has suggested no role for anticoagulation therapy such as low molecular weight heparin or low-dose aspirin in the treatment of RPL, the selection of appropriate patients using SNP analysis might enhance the therapeutic efficacy of such treatments (Kaandorp *et al.*, 2010). Targeted drug delivery technologies might also yield more effective yet safer chemotherapeutics for RPL in the future.

Authors' roles

H.M. played a role in execution, analysis, manuscript drafting and critical discussion. H.N. was involved in analysis, manuscript drafting and critical discussion; S.O., M.S., A.I., H.E., S.N., T.K. and K.P.-K. contributed to execution and analysis. I.N., T.F. and Y.I. played a role in execution, analysis and crtical discussion. A.M., I.Y. and Y.U. were involved in study design and critical discussion. H.K. contributed to study design, manuscript drafting and critical discussion.

Acknowledgements

The authors thank Drs T. Sawada, Y. Nishiyama, E. Kitaoka, M. Yoshida, K. Tsukada, A. Nakamura and T. Koishi for providing samples. The authors also thank Dr T. Kishi for technical assistance and Dr Y. Onouchi for helpful discussions.

Funding

This study was supported by a grant-in-aid for Scientific Research from the Ministry of Education, Culture, Sports, Science and Technology of Japan (to H.K.).

References

Bogdanova N, Horst J, Chlystun M, Croucher PJ, Nebel A, Bohring A, Todorova A, Schreiber S, Gerke V, Krawczak M *et al.* A common haplotype of the annexin A5 (ANXA5) gene promoter is associated with recurrent pregnancy loss. *Hum Mol Genet* 2007;**16**:573–578.

Bolor H, Mori T, Nishiyama S, Ito Y, Hosoba E, Inagaki H, Kogo H, Ohye T, Tsutsumi M, Kato T *et al.* Mutations of the SYCP3 gene in women with recurrent pregnancy loss. *Am J Hum Genet* 2009;**84**:14–20.

Chinni E, Tiscia GL, Colaizzo D, Vergura P, Margaglione M, Grandone E. Annexin V expression in human placenta is influenced by the carriership of the common haplotype M2. *Fertil Steril* 2009;**91**:940–942.

Coulam CB, Jeyendran RS, Fishel LA, Roussev R. Multiple thrombophilic gene mutations rather than specific gene mutations are risk factors for recurrent miscarriage. *Am J Reprod Immunol* 2006;**55**:360–368.

Gerke V, Moss SE. Annexins: from structure to function. *Physiol Rev* 2002; **82**:331–371.

Grandone E, Tiscia G, Colaizzo D, Vergura P, Pisanelli D, Margaglione M. The haplotype M2 within the ANXA5 gene is independently associated with the occurrence of deep venous thrombosis. *Thromb Haemost* 2010a;**103**:1102–1103.

Grandone E, Tiscia G, Colaizzo D, Chinni E, Pisanelli D, Bafunno V, Margaglione M. Role of the M2 haplotype within the annexin A5 gene in the occurrence of pregnancy-related venous thromboembolism. *Am J Obstet Gynecol* 2010b;**203**:461.e1–5.

Kaandorp SP, Goddijn M, van der Post JA, Hutten BA, Verhoeve HR, Hamulyák K, Mol BW, Folkeringa N, Nahuis M, Papatsonis DN *et al.*

Aspirin plus heparin or aspirin alone in women with recurrent miscarriage. *N Engl J Med* 2010;**362**:1586–1596.

Krikun G, Lockwood CJ, Wu XX, Zhou XD, Guller S, Calandri C, Guha A, Nemerson Y, Rand JH. The expression of the placental anticoagulant protein, annexin V, by villous trophoblasts: immunolocalization and *in vitro* regulation. *Placenta* 1994;**15**:601–612.

Rai R, Regan L. Recurrent miscarriage. *Lancet* 2006;**368**:601–611.

Rand JH. The annexinopathies: a new category of diseases. *Biochim Biophys Acta* 2000;**1498**:169–173.

Rand JH, Wu XX, Andree HA, Lockwood CJ, Guller S, Scher J, Harpel PC. Pregnancy loss in the antiphospholipid-antibody syndrome–a possible thrombogenic mechanism. *N Engl J Med* 1997; **337**:154–160.

Shapiro SS. The lupus anticoagulant/antiphospholipid syndrome. *Annu Rev Med* 1996;**47**:533–553.

Sierra S, Stephenson M. Genetics of recurrent pregnancy loss. *Semin Reprod Med* 2006;**24**:17–24.

Tiscia G, Colaizzo D, Chinni E, Pisanelli D, Sciannamè N, Favuzzi G, Margaglione M, Grandone E. Haplotype M2 in the annexin A5 (ANXA5) gene and the occurrence of obstetric complications. *Thromb Haemost* 2009;**102**:309–313.

Wang X, Campos B, Kaetzel MA, Dedman JR. Annexin V is critical in the maintenance of murine placental integrity. *Am J Obstet Gynecol* 1999; **180**:1008–1016.

Ward KJ. Genetic factors in recurrent pregnancy loss. *Semin Reprod Med* 2000;**18**:425–432.

RESEARCH LETTER

Relationship between heat-induced fibrillogenicity and hemolytic activity of thermostable direct hemolysin and a related hemolysin of Vibrio parahaemolyticus

Kiyouhisa Ohnishi[1], Kumiko Nakahira[1], Satoru Unzai[2], Kouta Mayanagi[3], Hiroshi Hashimoto[2], Kentaro Shiraki[4], Takeshi Honda[5] & Itaru Yanagihara[1]

[1]Department of Developmental Medicine, Osaka Medical Center for Maternal and Child Health, Research Institute, Osaka, Japan; [2]Supramolecular Biology, Graduate School of Nanobioscience, Yokohama City University, Yokohama, Japan; [3]Medical Institute of Bioregulation, Kyushu University, Institute for Bioinformatics Research and Development, Japan Science and Technology Agency, Fukuoka, Japan; [4]Institute of Applied Physics, University of Tsukuba, Ibaraki, Japan; and [5]Department of Bacterial Infections, Research Institute for Microbial Diseases, Osaka University, Osaka, Japan

Correspondence: Itaru Yanagihara, Department of Developmental Medicine, Research Institute, Osaka Medical Center for Maternal and Child Health, 840 Murodo-cho, Izumi, Osaka 594-1101, Japan. Tel.: +81 725 56 1220; fax: +81 725 57 3021; e-mail: itaruy@mch.pref.osaka.jp

Received 27 October 2010; revised 13 January 2011; accepted 25 January 2011.

DOI:10.1111/j.1574-6968.2011.02233.x

Editor: Ian Henderson

Keywords
thermostable direct hemolysin-related hemolysin; fibrillogenicity; tetrameric structure; Arrhenius effect.

Abstract

The formation of nonspecific ion channels by small oligomeric amyloid intermediates is toxic to the host's cellular membranes. Thermostable direct hemolysin (TDH) and TDH-related hemolysin (TRH) are major virulence factors of *Vibrio parahaemolyticus*. We have previously reported the crystal structure of TDH tetramer with the central channel. We have also identified the molecular mechanism underlying the paradoxical responses to heat treatment of TDH, known as the Arrhenius effect, which is the reversible amyloidogenic property. In the present report, we describe the biophysical properties of TRH, which displays 67% amino acid similarity with TDH. Molecular modeling provided a good fit of the overall structure of TDH and TRH. Size-exclusion chromatography, ultracentrifugation, and transmission electron microscopy revealed that TRH formed tetramer in solution. These toxins showed similar hemolytic activity on red blood cells. However, TRH had less amyloid-like structure than TDH analyzed by thioflavin T-binding assay and far-UV circular dichroism spectra. These data indicated that amyloidogenicity upon heating is not essential for the membrane disruption of erythrocytes, but the maintenance of tetrameric structure is indispensable for the hemolytic activity of the TDH and TRH.

Introduction

Vibrio parahaemolyticus is a gram-negative marine bacterium recognized as a major cause of seafood-borne gastroenteritis around the world. Wound infections, septicemia, and other infections are also caused occasionally by *V. parahaemolyticus* outbreaks (Blake *et al.*, 1980; Daniels *et al.*, 2000). Thermostable direct hemolysin (TDH) and its homolog TRH are the major virulence factors of this microorganism (Honda *et al.*, 1980, 1988; Joseph *et al.*, 1982; Shirai *et al.*, 1990). TDH and TRH have various biological activities in common, being hemolytic, cardiotoxic, lethal, and enterotoxic (Honda & Iida, 1993; Raimondi *et al.*, 2000; Naim *et al.*, 2001). Mature forms of TDH and TRH consist of 165 amino acids with a pair of intramolecular disulfide bonds between cysteine moieties in positions 151 and 161 (Iida & Honda, 1997). TDH-positive *V. parahaemolyticus* is hemolytic on Wagatsuma agar, which is a special type of blood agar; this effect is known as the Kanagawa phenomenon (Miwatani *et al.*, 1972; Okuda & Nishibuchi, 1998). Electron microscopic observations indicated that TDH formed pore-like structures on the surface of erythrocyte membranes (Honda *et al.*, 1992). Furthermore, when lipid bilayers were treated with TDH, single channel pore formation was observed (Hardy *et al.*, 2004). In addition, Miwatani reported that heating crude TDH at 60 °C inactivated its hemolytic activity but the activity was restored by rapid cooling from the denatured state at 90 °C (Miwatani *et al.*, 1972). This paradoxical phenomenon is known as the Arrhenius effect, which was originally reported with the α-hemolysin of *Staphylococcus aureus* by S.A. Arrhenius in 1907 (Arrhenius, 1907). We have previously determined that the underlying molecular mechanism mediating the Arrhenius

effect in TDH is the reversibility of amyloid fibril formation upon heating of TDH (Fukui *et al.*, 2005). On the other hand, TRH lost its hemolytic activity upon heating at 90 °C, suggesting that TRH activity is not associated with the Arrhenius effect in the same way as TDH (Honda *et al.*, 1988). We have also previously identified the C_4-symmetric tetrameric structure of TDH and its model in low solutions using small-angle X-ray scattering, ultracentrifugation, and transmission electron microscopy (Hamada *et al.*, 2007), and presented the crystal structure of TDH tetramers with a central pore at a 1.5 Å resolution (Yanagihara *et al.*, 2010). Single amino acid substitutions of TDH showed that π-cation interactions between R46 and Y140 played an important role in maintaining the tetrameric structure, whereas the monomeric mutant, R46E, lost its hemolytic activity (Yanagihara *et al.*, 2010). TRH shares antigenicity in part with TDH. Hybridization tests with *trh* gene-specific probes showed that *trh* gene had nucleotide sequence variations, *trh1* and *trh2* gene, in clinical strains (Nishibuchi *et al.*, 1989; Kishishita *et al.*, 1992). The *trh1* gene is 84% homologous to the *trh2* gene, and its nucleotide sequence analysis indicated that it shares 68% homology with *tdh* gene. The amino acid sequence of *trh1* gene also shares 63% homology with that of *tdh* gene (Nishibuchi *et al.*, 1989). However, detailed structural analysis and the association state of native TRH remain unclear.

Protein aggregation and amyloid formation are related to many protein conformational diseases, including Alzheimer's, Huntington's, and Parkinson's disease (Bucciantini *et al.*, 2002; Quist *et al.*, 2005). Following appropriate conditions, a number of disease- and non-disease-associated proteins undergo amyloid fibril formation *in vitro* (Uversky & Fink, 2004). Amyloid fibrils are rich in β-sheet and can be observed with thioflavin T (ThT) assay or by staining with Congo red, indicating that they contain a hydrophobic region. Although these fibrillar amyloids were previously considered to be the primary factor in the induction of pathology in these protein conformational diseases, recent studies indicate that small oligomers or protofibrils, rather than amyloid fibrils, may play an important role in cytotoxicity (Lesné *et al.*, 2006; Haataja *et al.*, 2008).

In this study, we compared TDH and TRH to investigate whether membrane toxicity by the toxins is induced by amyloidogenicity upon heating or small oligomerized tetrameric structures. TRH showed less amyloidogenicity compared with that of TDH. However, the hemolytic activity of TRH was similar to that of TDH. These data indicate that membrane disruption by the TDH family is mediated by tetrameric structures and not by the amyloidogenicity. We also compared the circular dichroism (CD) spectra of TDH and TRH in the heat-denatured state and found that an incorrect refolding process resulted in loss of the Arrhenius effect of TRH.

Materials and methods

Purification of recombinant proteins and hemolytic assay

Purification of recombinant TDH was performed as described previously (Naim *et al.*, 2001). N-terminal signal peptide-deleted (1–24 amino acids) *trh1* (GenBank accession no. AB112353) was inserted into the expression vector pET-28a (Novagen). For the expression of recombinant TRH, we transformed a plasmid vector pET28-a harboring *trh1* gene into *Escherichia coli* JM109 (DE3) cells (Promega). The transformant was cultured in Luria–Bertani broth (1% Bacto tryptone, 0.5% yeast extract, and 1% NaCl) containing 100 μg mL^{-1} of kanamycin at 30 °C for 30 h with rotary shaking, and then centrifuged at 6000 *g* for 30 min. We added ammonium sulfate (55% saturation) to the supernatant and allowed it to stir overnight, followed by centrifugation at 10 000 *g* for 1 h. The pellet was dissolved in 10 mM phosphate buffer (pH 7.4) and dialyzed against the same buffer. We applied this solution to a series of columns: Cellulofine Hap (hydroxyapatite) (Seikagaku-Kogyo, Tokyo, Japan), Toyopearl DEAE-650M (Tosoh, Tokyo, Japan), Resource-Phe (Amersham Pharmacia Biotech AB, Uppsala, Sweden), and Superose 6 (GE Healthcare, Uppsala, Sweden). Hemolytic activities were measured as described previously (Fukui *et al.*, 2005).

CD spectrum

Far-UV CD spectra were recorded with a J-720W spectropolarimeter (Jasco, Tokyo, Japan) equipped with a thermoelectric temperature controller. Data were analyzed with the software provided by Jasco. Measurements were taken in a quartz cuvette with a path length of 2 mm, scanned in steps of 0.2 nm at a rate of 50 nm min^{-1}. Samples of 0.2 mg mL^{-1} TRH in 10 mM phosphate buffer (pH 7.4) were heated up from 37 to 90 °C at a heating rate of 0.1 °C min^{-1}. After heat treatment at 90 °C, the temperature was decreased rapidly by 30 °C min^{-1} or slowly by 1 °C min^{-1} decrements to 37 °C. Data were analyzed by molar residue ellipticity [θ], defined as $[\theta] = 100\theta_{obs}/cl$ (deg cm^2 dmol^{-1}), where θ_{obs} is observed ellipticity in degrees and c and l are the concentration (mol L^{-1}) of protein residue and the light pass is in cm, respectively. Secondary structures of TDH and TRH were predicted from CD data using the CDPRO program package (Sreerama & Woody, 2000). The CDPRO suite contains modified versions of three methods: SELCON3, CONTINLL, and CDSSTR. All methods are based on comparison of the far-UV CD spectrum of the protein undergoing testing with CD spectra of reference proteins with a known three-dimensional structure. Using three methods and one set of reference proteins, we obtained the predicted secondary structures.

Analytical ultracentrifugation

We performed analytical ultracentrifugation experiments using an Optima XL-1 analytical ultracentrifuge (Beckman Coulter, Fullerton, CA) with a Beckman An-50 Ti rotor. Sedimentation equilibrium experiments were carried out in cells with a six-channel centerpiece and quartz windows. The sample concentrations used were 0.15, 0.31, and 0.59 mg mL^{-1} dissolved in 10 mM phosphate buffer (pH 7.4) and 100 mM NaCl. We set the absorbance wavelength at 280 nm. Data were obtained at 2600 *g* (6000 rpm) and 5900 *g* (9000 rpm) at 20 °C.

A total equilibration time of 22 h was used for each speed, with a scan taken at 18 h to ensure that equilibrium had been reached. We calculated the partial specific volume of the protein, solvent density, and solvent viscosity from standard tables using the program SEDNTERP (version 1.09). Data analysis was performed by global analysis of datasets obtained at different loading concentrations and rotor speeds using ULTRASPIN software (MRC Center for Protein Engineering, Cambridge, UK; http://www.mrc-cpe.cam.ac.uk/ultraspin).

Homology modeling

The homology model of TRH was built by the program MODELLER (Marti-Renom *et al.*, 2000) using the crystal structure of TDH (PDB: 3A57).

Transmission electron microscopy

Sample preparation was performed as described previously (Fukui *et al.*, 2005; Hamada *et al.*, 2007). We diluted samples containing 20 μg mL^{-1} TRH with 10 mM sodium phosphate (pH 7.4). For negative staining, 4 μL of the solution was applied to a copper grid supporting a thin continuous carbon film, left for 1 min, and then stained with three drops of 2% uranyl acetate. Images were recorded by a BioScan CCD camera (Gatan) with a pixel size of 3.1 Å, using a JEM1010 electron microscope (Jeol, Tokyo, Japan).

Kinetics of fibril formation with ThT assay

We incubated protein samples (0.2 mg mL^{-1}) with 10 μM ThT in 50 mM glycine–NaOH (pH 8.5) according to a previous report (Fukui *et al.*, 2005). Fluorescence of ThT was measured at 485 nm with an excitation wavelength of 450 nm using an FP-777 (Jasco) spectrofluorometer. The kinetic of fibril formation was described previously (Hamada & Dobson, 2002; Fukui *et al.*, 2005). Each kinetic traces was fitted to the stretched exponential function $F = F_{\infty} + \Delta F \exp[(-kt)^n]$. In this equation, F, F_{∞}, and ΔF are the fluorescence intensity at time t, the final fluorescence intensity and the fluorescence amplitude, respectively. The k and n value represent the rate constant per minute, the heterogenicity parameter.

Results and discussion

Purification of recombinant TRH

The predicted amino acid sequence similarity between the two recombinant toxins TRH and TDH used in this study was 67.3%. From 2 L of culture supernatant of JM109 (DE3) harboring the recombinant plasmid, a final amount of 6 mg signal peptide-deleted TRH was purified using a series of column chromatography procedures. Purified TRH showed a single band by sodium dodecyl sulfate-polyacrylamide gel electrophoresis. The molecular size of both purified TRH and purified TDH was 23 kDa. This molecular size of TRH is consistent with that estimated in a previous study on the purification of native TRH from *V. parahaemolyticus* clinical isolates (Honda *et al.*, 1988).

TRH forms tetrameric structure in solution

TDH forms tetramer in solution (Fukui *et al.*, 2005; Hamada *et al.*, 2007). We performed size-exclusion chromatography to investigate the association state of TRH in solution. The elution volume of TRH corresponded with that of tetrameric TDH, indicating that TRH is organized into a tetrameric structure (Fig. 1a). We investigated the association and equilibrium state of TRH by analytical ultracentrifugation (Fig. 1b). Sedimentation equilibrium showed that the molecular mass of TRH was 75 000 ± 200 Da, which is similar to the molecular mass of tetrameric TDH of 75 000 ± 700 Da as determined by sedimentation equilibrium analysis (Hamada *et al.*, 2007). The molecular mass of monomeric TRH was calculated as 18 600 Da. Therefore, TRH also exists as a tetramer in solution. Further, transmission electron microscopy of negatively stained samples showed tetrameric oligomerization of TRH (Fig. 1c). To investigate differences in structure and function between TRH and TDH at the atomic level, we built the homology model of TRH and compared the three-dimensional structures of TRH and TDH. The structure of TRH exhibited a good fit to that of TDH (Fig. 1d). Furthermore, the three-dimensional position of R46, E138, and Y140, which may participate in π-cation interactions and maintain TDH tetrameric structures, was also conserved in TRH, suggesting that they may be important factors for tetrameric structure and hemolysis for these toxins.

Hemolytic activity and amyloidogenicity of TDH and TRH

To compare the hemolytic activities of TRH and TDH, we measured their activities in human erythrocytes (Fig. 2a). At 1 μM, the hemolytic activity of TRH was higher than that of TDH. However, this difference was not observed when the concentration was > 4 μM.

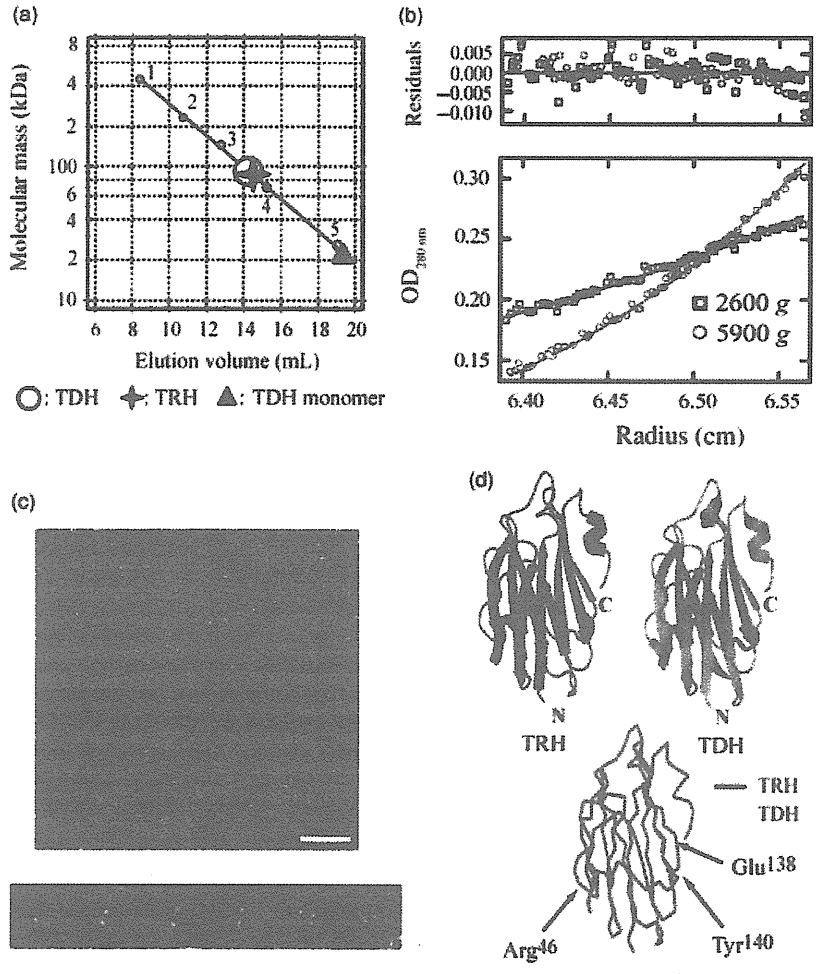

Fig. 1. Like TDH, TRH forms a tetramer in solution. (a) The molecular mass determination by size-exclusion analysis. The molecular size of recombinant TRH purified in this study was analyzed using Superose 6. The circle and star near 90 kDa represent tetrameric TDH and purified TRH. The other larger circle near 30 kDa is monomeric TDH (triangle). Small circles indicate molecular mass standards: (1) 440 kDa (ferritin); (2) 232 kDa (catalase); (3) 150 kDa (aldolase); (4) 67 kDa (albumin); (5) 25 kDa (chymotrypsinogen). (b) Sedimentation equilibrium of TRH. Circles and squares are samples ultracentrifuged at 2600 and 5900 *g*, respectively. Lines show the fitted curves using a single species model. The residuals represent the differences between the calculated fit and the experimental data. (c) Transmission electron microscopy of negatively stained TRH. TRH samples were stained with 2% uranyl acetate. The white bar represents 100 nm. Representative TRH molecule images are magnified below. (d) Construction of the molecular model for TRH. Homology model of TRH (green) and crystal structure of TDH (yellow). Arg^{46}, Glu^{138} and Tyr^{140} of TRH and TDH are shown by red.

To investigate whether TRH shows an Arrhenius effect, the hemolytic activity of TRH was measured after various heat treatments (Fig. 2b). TDH lost its hemolytic activity after heating at 60 °C for 30 min (TDH, fibril); however, the activity was recovered after rapid cooling from the denatured state at 90 °C (TDH, refold; the Arrhenius effect). TRH lost its hemolytic activity after heating at 60 °C for 30 min (TRH, heat), and the activity was not recovered even after rapid cooling from the denatured state at 90 °C (TRH, rapid cool). These results suggest that, unlike TDH, TRH does not exhibit the Arrhenius effect.

We have previously reported that heat inactivation of TDH at 60 °C is a result of structural conversion to heat-reversible amyloid fibril formations (Fukui *et al.*, 2005). To address the possibility that heat-induced TRH possesses amyloidogenic properties, TRH and TDH samples were measured by ThT (Fig. 2c; Supporting Information, Fig. S1). TDH showed high fluorescence, indicating that amyloids formed fibrils composed of cross-β-strands after heat treatment. In contrast, heat treatment of TRH resulted in lower ThT fluorescence compared with that of TDH. In addition, time course analysis of fluorescence intensity at 485 nm showed that the final fluorescence intensity F_∞ (arbitrary unit) of TDH and TRH was 76.5 and 26.8, respectively (Fig. 2d). Based on the ThT assay, TRH may have less amyloid-like structure than TDH. Amyloid fibrils are the pathological hallmark of protein conformational diseases, and considered critical to understanding the pathogenesis of these diseases (Hardy & Selkoe, 2002). Recent investigations have indicated that the essence of the pathogenic agent is not amyloid fibril but a small species, perhaps consisting of channel-forming oligomers that might form in association with membranes (Quist *et al.*, 2005; Jang *et al.*, 2010). Our previous electron microscopic observations showed that TDH tetramer attached diagonally to the liposome membrane by maintaining its tetrameric structure (Yanagihara *et al.*, 2010). In fact, in this study, both TDH and TRH lost their hemolytic activity after amyloid fibril formation upon heating, as confirmed by ThT assay. Although TRH had lower amyloidogenicity than TDH, its

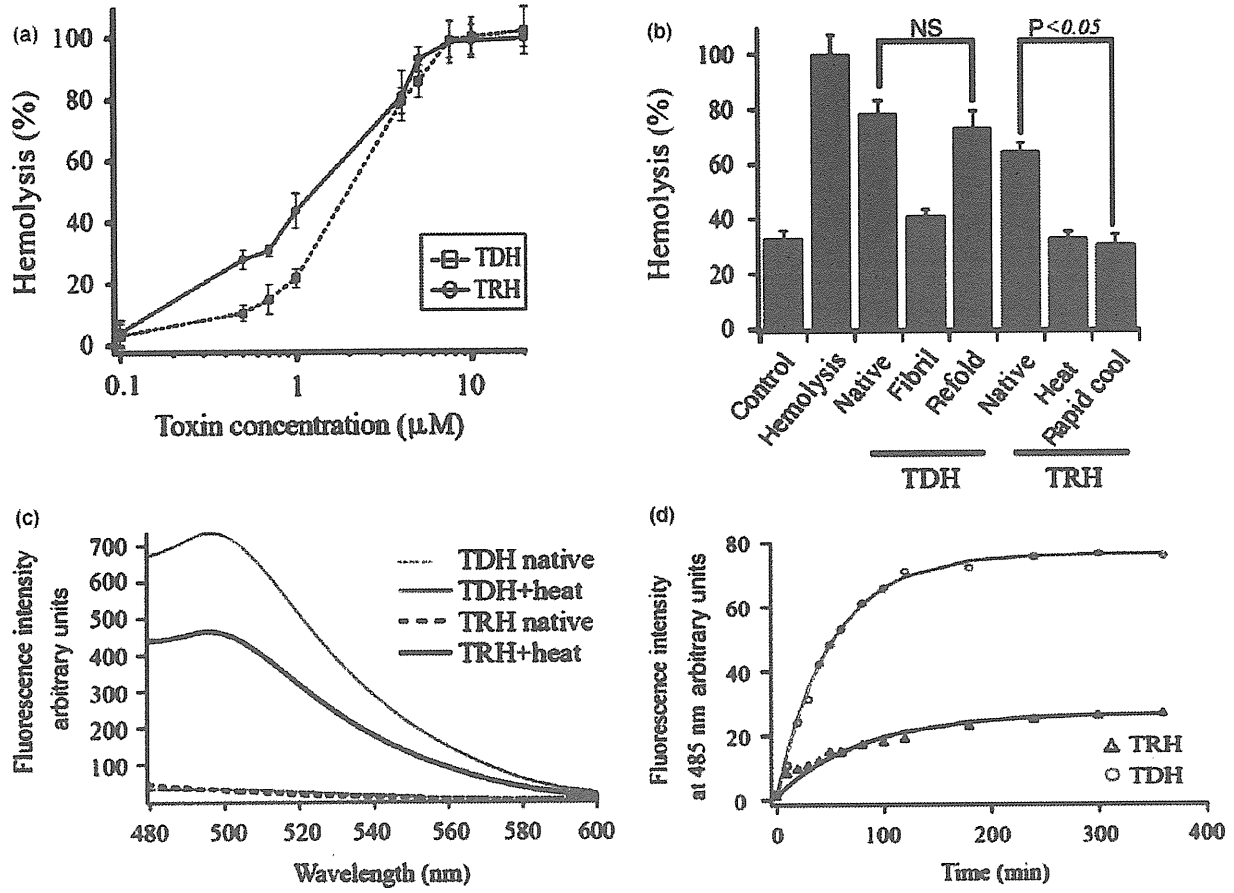

Fig. 2. Hemolytic activity and ThT assay of TRH and TDH. (a) Hemolytic activities of TDH and TRH on 2% human erythrocyte in phosphate-buffered saline (PBS). TDH (squares and dotted line) or TRH (circles and line) was incubated with human erythrocytes at 37 °C for 1 h and centrifuged. Its supernatant was measured with a spectrophotometer. (b) Hemolytic activities of TDH and TRH after various heat treatments. Samples (5 μM) treated with PBS (control) or 2% Triton X-100 (hemolysis) indicate negative and positive controls, respectively. The data represent the mean values ± SD of five independent experiments. Samples at 37 °C (native), samples at 60 °C (fibril for TDH, heat for TRH), and samples with rapid cooling (30 °C min^{-1}) after denaturation at 90 °C (refold for TDH, rapid cool for TRH). (c) Fibrillogenic ability of TRH and TDH. Samples (0.2 mg mL^{-1}) were incubated with 5 μM ThT in 50 mM glycine–NaOH (pH 8.5) and the fluorescence was measured by spectrofluorometer. The measured samples are TRH in native state, TRH after being heated at 60 °C for 30 min, TDH in native state, and TDH with the same heat treatment as TRH. (d) Time-dependent fibril formation of TRH and TDH. Each sample was incubated in 55 °C and the fluorescence intensity at 485 nm was measured at each time. The results for TRH and TDH are the average of triplicate experiments.

hemolytic activity closely corresponded to that of TDH, suggesting that tetrameric structure, and not amyloid fibrils, played an important role in hemolytic activity.

Far-UV and secondary structure contents of TRH upon heating

The Arrhenius effect of TDH is explained by correct refolding of TDH from its heat-denatured state back to its native structure (Fukui *et al.*, 2005). We therefore examined conformational changes in TRH following heat denaturation. First, we measured the far-UV spectrum of native TRH upon heating. Far-UV CD spectra of TRH showed gradual unfolding of the protein structure upon heating from 55 to 90 °C (Fig. 3a). Next, we compared the far-UV spectra in the denatured state to the spectra obtained after rapid cooling (30 °C min^{-1}, Fig. 3b) and slow cooling (1 °C min^{-1}, Fig. 3c). The far-UV spectra of TRH after rapid and after slow cooling were different from that of native TRH, indicating that TRH lost its ability to refold correctly from the denatured state. The secondary structure contents of TRH and TDH are shown in Table 1. Interestingly, the α-helix content of TDH recovered after rapid cooling from the heat-denatured state, whereas the α-helix content of TRH diminished after rapid cooling following the same treatment. This result suggests that correct refolding of α-helix structure in

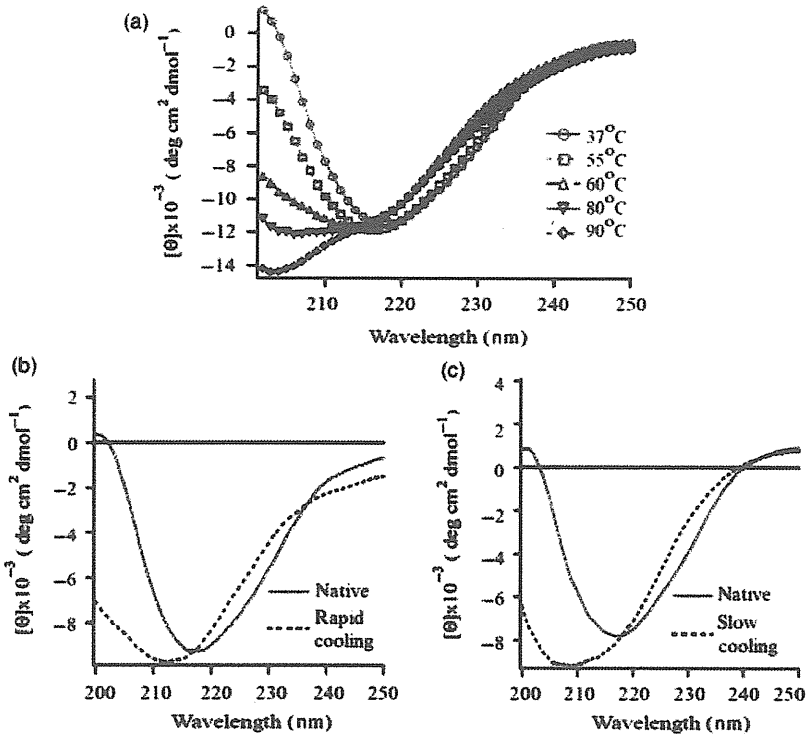

Fig. 3. Far-UV CD spectra of TRH upon heating. CD spectra of TRH samples with various heat treatments (a), after denaturation followed by rapid cooling (b), and after slow cooling (c).

the TDH and TRH is important for stabilization of the tetrameric native structure to avoid nonspecific protein aggregation. For instance, during the refolding process, β-lactoglobulin refolded into a specific state rich in α-helix before β-sheet formation in the denatured state (Shibayama, 2008). The incorrect refolding of TRH α-helix from the denatured state might disturb the entire protein structure and function of TRH. Alternatively, maintenance of TRH α-helix structure contents after heat denaturation may be related to the structural stability of the amyloidogenic proteins. Further investigations at atomic level are needed to clarify whether the correct refolding of α-helix contents from the denatured state is essential for the Arrhenius effect.

Our findings indicated that the TDH and TRH showed similar hemolytic activity *in vitro*. Previous reports showed that the expression level of the *trh* gene (Kanagawa phenomenon-negative strains) is much lower than that of the *tdh* gene (Kishishita *et al.*, 1992; Okuda & Nishibuchi, 1998). These data may also account for the epidemiological finding that larger numbers of patients with TDH-positive strains are reported among the *V. parahaemolyticus* infections in contrast to those with TRH-positive strains. In this study, we used human red blood cells for bioassay because the Kanagawa phenomenon is the most classical and distinguishable biological assay for TDH-positive and TRH-positive clinical strains. However, TDH is reported to show cytotoxicity on various mammalian cell lines, including intestinal cells. To clarify the entire process of the pathobiology of TDH and TRH, including its amyloidogenic/aggregative properties upon heating or in a hydrophobic membranous environment, future studies will be needed.

Table 1. The secondary structure contents of TDH and TRH in various states

		Secondary structure contents (%)		
Hemolysin	State*	α-Helix	β-Sheet	Turn&Unrd†
TDH	Native	20.2 ± 0.6	23.8 ± 3.0	56.3 ± 4.0
	Denatured	15.1 ± 4.8	27.0 ± 3.4	57.9 ± 5.0
	Refolded	18.1 ± 1.5	25.0 ± 2.0	57.8 ± 8.0
TRH	Native	23.1 ± 1.4	25.4 ± 3.7	52.0 ± 2.8
	Denatured	17.6 ± 5.5	24.5 ± 2.9	56.0 ± 3.4
	Refolded	10.0 ± 3.3	28.0 ± 3.4	62.0 ± 6.2

*Native, samples at 37 °C; denatured, samples at 90 °C; refolded, rapid cooling (30 °C min^{-1}) samples from denatured state.
†Turn&Unrd, unordered structure.

Acknowledgements

We are grateful to Dr Takashi Fukui (Laboratory of Microbiology and Immunology, Faculty of Pharmacy, Chiba Institute of Science) for participating in valuable discussions. This study was supported in part by grants-in-aid from the Ministry of Education, Culture, Sports, Science and Technology (MEXT), Japan; Ministry of Health, Labor and Welfare, Japan; The Foundation for Mother and Child

Well-being, Osaka, Japan; and Osaka Research Society for Pediatric Infectious Disease, Osaka, Japan.

References

Arrhenius S (1907) *Immunochemie. Anwendungen der physikalischen Chemie auf die Lehre von den physiologichen Antikoerpern.* Akademische Verlagsgesellschaft, Leipzig.

Blake PA, Weaver RE & Hollis DG (1980) Diseases of humans (other than cholera) caused by vibrios. *Annu Rev Microbiol* **34**: 341–367.

Bucciantini M, Giannoni E, Chiti F, Baroni F, Formibli L, Zurdo J, Taddei N, Ramponi G, Dobson CM & Stefani M (2002) Inherent toxicity of aggregates implies a common mechanism for protein misfolding diseases. *Nature* **416**: 507–511.

Daniels NA, Mackinnon L, Bishop R *et al.* (2000) *Vibrio parahaemolyticus* infections in the United States, 1973–1998. *J Infect Dis* **181**: 1661–1666.

Fukui T, Shiraki K, Hamada D *et al.* (2005) Thermostable direct hemolysin of *Vibrio parahaemolyticus* is a bacterial reversible amyloid toxin. *Biochemistry* **44**: 9825–9832.

Haataja L, Gurlo T, Huang CJ & Butler PC (2008) Islet amyloid in type 2 diabetes, and the toxic oligomer hypothesis. *Endocr Rev* **29**: 303–316.

Hamada D & Dobson CM (2002) A kinetic study of β-lactoglobulin amyloid fibril formation promoted by urea. *Protein Sci* **11**: 2411–2426.

Hamada D, Higurashi T, Mayanagi K, Miyata T, Fukui T, Iida T, Honda T & Yanagihara I (2007) Tetrameric structure of thermostable direct hemolysin from *Vibrio parahaemolyticus* revealed by ultracentrifugation, small-angle X-ray scattering and electron microscopy. *J Mol Biol* **365**: 187–195.

Hardy J & Selkoe DJ (2002) The amyloid hypothesis of Alzheimer's disease: progress and problems on the road to therapeutics. *Science* **297**: 353–356.

Hardy PS, Nakano M & Iida T (2004) Single channel evidence for innate pore-formation by *Vibrio parahaemolyticus* thermostable direct haemolysin (TDH) in phospholipid bilayers. *FEMS Microbiol Lett* **240**: 81–85.

Honda T & Iida T (1993) The pathogenicity of *Vibrio parahaemolyticus* and the role of the thermostable direct hemolysin and related hemolysin. *Rev Med Microbiol* **4**: 106–113.

Honda T, Chearskul S, Takeda Y & Miwatani T (1980) Immunological methods for detection of Kanagawa negative *Vibrio parahaemolyticus*. *Lancet* **i**: 331–332.

Honda T, Ni Y & Miwatani T (1988) Purification and characterization of a hemolysin produced by a clinical isolated of Kanagawa phenomenon-negative *Vibrio parahaemolyticus* and related to the thermostable direct hemolysin. *Infect Immun* **56**: 961–965.

Honda T, Ni Y & Miwatani T (1992) The thermostable direct hemolysin of *Vibrio parahaemolyticus* is a pore-forming toxin. *Can J Microbiol* **38**: 1175–1180.

Iida T & Honda T (1997) Hemolysins produced by *Vibrios*. *J Toxicol-Toxin Rev* **16**: 215–227.

Jang H, Arce FT, Ramachandran S, Capone R, Azimova R, Kagan BL, Nussinov R & Lal R (2010) Truncated beta-amyloid peptide channels provide an alternative mechanism for Alzheimer's disease and Down syndrome. *P Natl Acad Sci USA* **107**: 6538–6543.

Joseph SW, Colwell RR & Kaper JB (1982) *Vibrio parahaemolyticus* and related halophilic vibrios. *Crit Rev Microbiol* **10**: 77–124.

Kishishita M, Matsuoka N, Kumagai K, Yamasaki S, Takeda Y & Nishibuchi M (1992) Sequence variation in the thermostable direct hemolysin-related hemolysin (*trh*) gene of *Vibrio parahaemolyticus*. *Appl Environ Microb* **58**: 2449–2457.

Lesné S, Koh MT, Kotilinek L, Kayed R, Glabe CG, Yang A, Gallagher M & Ashe KH (2006) A specific amyloid-beta protein assembly in the brain impairs memory. *Nature* **440**: 352–357.

Marti-Renom MA, Stuart AC, Fiser A, Sanchez R, Melo F & Sali A (2000) Comparative protein structure modeling of genes and genomes. *Annu Rev Bioph Biom* **29**: 291–325.

Miwatani T, Takeda Y, Sakurai J, Yoshihara A & Taga S (1972) Effect of heat (Arrhenius effect) on crude hemolysin of *Vibrio parahaemolyticus*. *Infect Immun* **6**: 1031–1033.

Naim R, Yanagihara I, Iida T & Honda T (2001) *Vibrio parahaemolyticus* thermostable direct hemolysin can induce an apoptotic cell death in Rat-1 cells from inside and outside of the cells. *FEMS Microbiol Lett* **195**: 237–244.

Nishibuchi M, Taniguchi T, Misawa T, Khaeomanee-Iam V, Honda T & Miwatani T (1989) Cloning and nucleotide sequence of the gene (*trh*) encoding the hemolysin related to the thermostable direct hemolysin of *Vibrio parahaemolyticus*. *Infect Immun* **57**: 2691–2697.

Okuda J & Nishibuchi M (1998) Manifestation of the Kanagawa phenomenon, the virulence-associated phenotype, of *Vibrio parahaemolyticus* depends on a particular single base change in the promoter of the thermostable direct haemolysin gene. *Mol Microbiol* **30**: 499–511.

Quist A, Doudevski I, Lin H, Azimova R, Ng D, Frangione B, Kagan B, Ghiso J & Lal R (2005) Amyloid ion channels: a common structural link for protein-misfolding disease. *P Natl Acad Sci USA* **102**: 10427–10432.

Raimondi F, Kao JPY, Fiorentini C, Fabbri A, Donelli G & Gasparini N (2000) Enterotoxicity and cytotoxicity of *Vibrio parahaemolyticus* thermostable direct hemolysin *in vitro* systems. *Infect Immun* **68**: 3180–3185.

Shibayama N (2008) Circular dichroism study on the early folding events of β-lactoglobulin entrapped in wet silica gels. *FEBS Lett* **582**: 2668–2672.

Shirai H, Ito H, Hirayama T, Nakamoto Y, Nakabayashi N, Kumagai K, Takeda Y & Nishibuchi M (1990) Molecular epidemiologic evidence for association of thermostable direct hemolysin (TDH) and TDH-related hemolysin of *Vibrio parahaemolyticus* with gastroenteritis. *Infect Immun* **58**: 3568–3573.

Sreerama N & Woody RW (2000) Estimation of protein secondary structure from circular dichroism spectra: comparison of CONTIN, SELCON, and CDSSTR methods with an expanded reference set. *Anal Biochem* **287**: 252–260.

Uversky VN & Fink AL (2004) Conformational constraints for amyloid fibrillation: the importance of being unfolded. *Biochim Biophys Acta* **1698**: 131–153.

Yanagihara I, Nakahira K, Yamane T *et al.* (2010) Structure and functional characterization of *Vibrio parahaemolyticus* thermostable direct hemolysin. *J Biol Chem* **285**: 16267–16274.

Supporting Information

Additional Supporting Information may be found in the online version of this article:

Fig. S1. Each 0.1 mg mL^{-1} TDH (A), TRH (B), concanavalin A at pH 5.1 (C) and pH 7.4 (D) was incubated for 20 min at the respective temperature. ThT fluorescence was measured according to the procedures described in Materials and methods.

Please note: Wiley-Blackwell is not responsible for the content or functionality of any supporting materials supplied by the authors. Any queries (other than missing material) should be directed to the corresponding author for the article.

The American Journal of Pathology, Vol. 178, No. 2, February 2011

DOI: 10.1016/j.ajpath.2010.10.005

Biomarkers, Genomics, Proteomics, and Gene Regulation

Reduced Stathmin-1 Expression in Natural Killer Cells Associated with Spontaneous Abortion

Yi Lin,* Cui Li,† Bin Shan,‡ Wenjing Wang,§ Shigeru Saito,¶ Jiehan Xu,* Jingfang Di,§ Yanmin Zhong,§ and Da-Jin Li‖**

From the Department of Obstetrics and Gynecology, Institute of Obstetrics and Gynecology, Renji Hospital, School of Medicine, Shanghai Jiaotong University, Shanghai; the Key Laboratory of Cancer Proteomics of Chinese Ministry of Health,† Xiangya Hospital, Central South University, Changsha, Hunan, China; the Department of Medicine,‡ Tulane University Health Sciences Center, New Orleans, Louisiana; the Institute of Tissue Transplantation and Immunology,§ College of Life Science and Technology, Jinan University, Guangzhou, China; the Department of Obstetrics and Gynecology,¶ Faculty of Medicine, University of Toyama, Toyama, Japan; the Laboratory for Reproductive Immunology,‖ Hospital and Institute of Obstetrics and Gynecology, Fudan University Shanghai Medical College, Shanghai, China; and the Department of Obstetrics and Gynecology,** Hainan Medical College Affiliated Hospital, Haikou, Hainan, China*

Female CBA/J mice impregnated by male DBA/2J mice (CBA/J×DBA/2J matings) are prone to spontaneous abortion, although the reason for this is unclear. In this study, the stathmin-1 expression pattern was evaluated in uterine natural killer (uNK) cells purified from CBA/J×DBA/2J matings. Results were compared with those in a CBA/J×BALB/c control group that yields successful pregnancies. The mean ± SD percentage of stathmin-1$^+$ cells in the CD49b$^+$ uNK cell population was lower in CBA/J×DBA/2J mice (0.7% ± 0.4%) than in control CBA/J×BALB/c mice (4.9% ± 1.5%, $P < 0.01$) using flow cytometry, and the intracellular stathmin-1 level in uNK cells was lower in CBA/J×DBA/2J mice than in control mice using Western blot analysis. Co-localization of lectin from Dolichos biflorus agglutinin (DBA-lectin) and stathmin-1 was confirmed using multivision immunohistochemical analysis. The frequency of stathmin-1$^+$DBA-lectin$^+$ cells was lower in CBA/J×DBA/2J mice than in CBA/J×BALB/c mice. A similar trend in the frequency of stathmin-1$^+$CD56$^+$ cells was seen in patients with unexplained spontaneous abortion compared with normal early pregnancy. A neutralizing antibody against stathmin-1 further increased the percentage of embryo loss in CBA/J×DBA/2J matings. These results provide evidence that stathmin-1 expression in uNK cells at the maternal-fetal interface may help modulate uNK cell function and may be beneficial for a successful pregnancy. ***(Am J Pathol 2011, 178:506–514; DOI: 10.1016/j.ajpath.2010.10.005)***

Stathmin-1 is a small (19-kDa) regulatory phosphoprotein that integrates diverse intracellular signaling pathways. It is highly conserved among vertebrates and is associated with tubulin binding and microtubule destabilization.[1,2] Stathmin-1 has a complex phosphorylation pattern in response to various extracellular signals, in particular growth and differentiation factors.[3] Moreover, stathmin-1 phosphorylation varies during the cell cycle.[4] It has thus been thought that stathmin-1 can act as a relay integrating the activation of diverse intracellular signaling pathways and mediating the control of cell proliferation, differentiation, and other functions.[5]

Stathmin-1 protein and mRNA were previously shown to be expressed in the pregnant uterus and decidualizing endometrial stromal cells in human and murine models.[6–8] Furthermore, stathmin-1 is up-regulated in rodent uteri at the site of embryo implantation and is highly

Supported by the National Natural Science Foundation of China (30730087, 30872761, and 30972970), the National Basic Research Program of China (2006CB944007), the Program for New Century Excellent Talents in University (NCET-07-0861), the Focus Construction Subject of Shanghai Education Department, the New Cutting-Edge Technology Project (SHDC12010122), a grant from the Ministry of Education, Culture, Sports, Science and Technology, Japan (Grant-in-Aid for Scientific Research [B] - 20390431), and grants from the Ministry of Health Labour and Welfare, Japan (Health Labour Sciences Research grant H20-kodomo-ippan-002).

Y.L., C.L., and B.S. contributed equally to this work.

Accepted for publication October 4, 2010.

Address reprint requests to Yi Lin, M.D., Department of Obstetrics and Gynecology, Institute of Obstetrics and Gynecology, Renji Hospital, School of Medicine, Shanghai Jiaotong University, Shanghai, 200001, China; or Da-Jin Li, M.D., Laboratory for Reproductive Immunology, Hospital and Institute of Obstetrics and Gynecology, Fudan University Shanghai Medical College, Shanghai, 200011, China. E-mail: yilinonline@gmail.com or djli@shmu.edu.cn.

expressed in the decidual zone during the decidualization process.[7,8] These results suggest that stathmin-1 may participate in the modulation of embryo implantation and decidualization.

Female CBA/J mice impregnated by male DBA/2J mice (CBA/J×DBA/2J matings) are prone to abortion, in contrast to the major histocompatibility complex–identical CBA/J×BALB/c matings, which are resistant to abortion.[9] The underlying mechanisms for these observations are unclear. Clark and colleagues[9] suggested that endothelium is the primary effector cell population, and this was supported by a recent work using CBA/J×DBA/2J matings.[10] Notably, inhibition of natural killer (NK) cells using anti-asialo GM1 antiserum significantly decreased the resorption rate of embryos in CBA/J×DBA/2J matings.[9] In the present study, uterine NK (uNK) cells were purified from CBA/J×DBA/2J and CBA/J×BALB/c allogeneic pregnant models using magnetic affinity cell sorting (MACS). The percentage of stathmin-1$^+$ cells in the uNK cell population was determined using flow cytometry, and the stathmin-1 protein expression level in uNK cells was determined using two-dimensional gel electrophoresis (2-DE), mass spectrometry (MS), and Western blot analysis. Multivision immunohistochemical analysis (IHC) was used to examine the distribution patterns of stathmin-1$^+$ cells in the uteri of pregnant female mice and in first-trimester human decidual tissue. In addition, inhibition of stathmin-1 was performed in CBA/J×DBA/2J, CBA/J×BALB/c, and CBA/J×CBA/J mice. From these data, the possible role of stathmin-1 in allogeneic pregnancy tolerance was investigated.

Materials and Methods

Pregnant Models of CBA/J×DBA/2J, CBA/J×BALB/c, and CBA/J×CBA/J Matings

Female CBA/J mice and male CBA/J, DBA/2J, and BALB/c mice (8 to 12 weeks old) were purchased from the Model Animal Center of Nanjing University (Nanjing, China) and were housed under specific pathogen-free conditions. Pregnant models of CBA/J×DBA/2J, CBA/J×BALB/c, and CBA/J×CBA/J matings were established by co-caging female CBA/J mice with DBA/2J, BALB/c, and CBA/J males, respectively. Detection of a vaginal plug was chosen to indicate day 0.5 of gestation (E0.5).[11,12] Embryonic day E12.5 was chosen as the gestational time to collect uNK cells because the uNK cells are at peak density on day E10 and have not yet begun to decrease in density through apoptosis (which begins on day E13 or E14).[13] Furthermore, we expected that it would be easier to distinguish healthy embryos from resorbing ones on day E12.5 than at an earlier time point. All animal procedures followed the national animal care guidelines, and associated data were approved for publication by the institutional review board of Shanghai Jiaotong University.

Purification of uNK Cells

Cell purification was performed by means of MACS.[11,12] Briefly, hysterolaparotomy was performed on day E12.5 to collect embryo-depleted placentas from CBA/J×DBA/2J and CBA/J×BALB/c matings. The uterine horns were opened longitudinally, and the fetoplacental unit was separated easily from the uterine implantation sites. The whole placental and decidual unit was separated individually from the respective embryo. The pooled placentas and decidua basalis (ie, decidual tissue in implantation sites) were collected into a dish and carefully cut into small pieces, collected in 0.9% NaCl solution, and subsequently filtered through a nylon mesh (50-μm pore size) to obtain a single cell suspension. Mononuclear cells were obtained by centrifuging of the single cell suspension using a Ficoll-Hipaque density column. Any red blood cells that contaminated the single cell suspension were eliminated by incubation with red blood cell lysis buffer (eBioscience Inc., San Diego, CA) two times at 37°C. Subsequently, NK cells were isolated using magnetic bead–conjugated antimouse CD49b monoclonal antibody, and CD49b$^+$ cells were purified by means of Mini MACS columns (Miltenyi Biotec Inc., Auburn, CA),[11,12] where CD49b was used as a common marker for murine NK cells.[14] The purity of the MACS-isolated NK cells routinely exceeded 95% as determined using flow cytometry.[12,15]

Flow Cytometry

Uterine NK cells were stained with phosphatidylethanolamine (PE)-conjugated antimouse CD49b (BioLegend, San Diego, CA) and rabbit anti–stathmin-1 (catalog number ab52906; Abcam, Cambridge, England) antibodies, followed by fluorescein isothiocyanate (FITC)–conjugated antirabbit IgG (Molecular Probes Inc., Eugene, OR). The percentage of stathmin-1$^+$ cells in the CD49b$^+$ NK cell population was determined by using a flow cytometer (FACSAria; BD Biosciences, Franklin Lakes, NJ).[11] Cells were stained with PE-conjugated antimouse CD49b and FITC-conjugated antimouse CD122 antibodies (both from BioLegend) to determine the percentage of CD122$^+$ cells in the CD49b$^+$ population. Isotype controls were established by using isotype control antibodies (BioLegend) to exclude false-positive cells. All the experiments were independently performed six times.[16–18]

Preparation of uNK Cell Lysates

Uterine NK cells were suspended in a modified radioimmunoprecipitation assay buffer [50 mmol/L Tris-HCl, pH 7.5, 150 mmol/L NaCl, 1% Triton X-100 (Roche Diagnostics GmbH, Mannheim, Germany), 1 mmol/L EDTA, 1 mmol/L phenylmethylsulfonyl fluoride, 0.66 μg/ml of aprotinin, 0.5 μg/ml of leupeptin, 1 μg/ml of pepstatin, 1 mmol/L Na_3VO_4, and 1 mmol/L NaF] and were sonicated three times for 5 seconds each. The cell lysates were centrifuged at 14,000 × *g* for 15 minutes at 4°C. The supernatants were collected, and their protein concen-

trations were measured by using the Bradford assay (Bio-Rad Laboratories, Hercules, CA).[19,20]

Two-Dimensional Gel Electrophoresis

The 2-DE was performed according to the manufacturer's instructions. Samples were loaded onto linear immobilized pH gradient (IPG) strips (IPGstrip, pH 4–7 L, 180 × 3 × 0.5 mm; Amersham Biosciences, Piscataway, NJ). Briefly, 1-mg protein samples were diluted to 350 μL with a rehydration solution [7 mol/L urea, 2 mol/L thiourea, 2% 3-([3-Cholamidopropyl]dimethylammonio)-l propanesulfonate, 18 mmol/L dithiothreitol, 0.5% (v/v) pH 4–7 IPG buffer, and trace bromophenol blue] and were applied to the IPG strips with 14 hours of rehydration at 30 V. The proteins were successively focused for 1 hour at 500 V, 1 hour at 1000 V, and 5 hours at 8000 V for a total of 41,920 V hours on an IPGphor (Amersham Biosciences). The focused IPG strips were equilibrated for 15 minutes in solution (6 mol/L urea, 2% SDS, 30% glycerol, 50 mmol/L Tris-HCl, pH 8.8, and 1% dithiothreitol) and then for an additional 15 minutes in the same solution containing 2.5% iodoacetamide instead of dithiothreitol. After equilibration, SDS–polyacrylamide gel electrophoresis was performed at 10°C on 10% SDS slab gels using the Ettan DALT II system (Amersham Biosciences) with the IPG strips sealed on the top of the gels with 0.5% agarose. An SDS–polyacrylamide gel electrophoresis was performed at a constant power of 2W/gel for 30 minutes and then switched to 12 W/gel until the bromophenol blue marker reached the bottom of the gel. Finally, the blue silver staining method (a modified Neuhoff's colloidal Coomassie Blue G-250 stain) was used to visualize the protein spots in the 2-DE gels.[17,20]

2-DE Image Data Analysis

Stained 2-DE gels were scanned using LabScan software and ImageScanner (Amersham Biosciences) at a solution of 300 dpi. Spot-intensity calibration, spot detection, matching, 1-D calibration, and establishment of an average gel were performed using the PDQuest System (Bio-Rad Laboratories). The theoretical molecular weight and pI value of the identified protein spots were calculated according to algorithms included in the PDQuest analysis software package. Significant differences in the protein expression levels were determined using the *t*-test, with significance defined at $P < 0.05$.[17,20]

Preparation of Protein Spots

Protein spots were excised from the preparative gels and were placed into a 96-well microtiter plate. Proteins were digested in gel as previously described.[17,20] The gel spots were destained using destaining solution [200 mmol/L NH_4HCO_3 and 100% acetonitrile (1:1)] for 20 minutes at room temperature. Gel spots were washed twice with deionized water, shrunk by dehydration in acetonitrile solution, and dried in a vacuum centrifuge. Samples were then swollen in a digestion buffer (20 mmol/L ammonium bicarbonate and 12.5 ng/μL of trypsin) (Sigma-Aldrich, St. Louis, MO) for 30 minutes at 4°C. The gels were then digested for 12 hours at 37°C. Tryptic peptides were extracted twice from the gel slices by sonication for 15 minutes in a 0.1% trifluoroacetic acid/50% acetonitrile solution. The supernatants were collected and dried to a pellet in a high-purity nitrogen flow. Peptides were eluted with 0.7 μL of α-cyano-4-hydroxycinnamic acid matrix solution and were loaded onto a stainless steel target with 192 wells (Applied Biosystems, Framingham, MA).[17,20]

Mass Spectrometry

Samples were air-dried and then were analyzed by using the Voyager System 4700 matrix-assisted laser desorption/ionization–time of flight–time of flight mass spectrometer (Applied Biosystems).[17,20]

Protein Identification

Known contaminating peaks (eg, keratin and autoproteolysis peaks) were removed before the database search. Spectra were processed and analyzed using a GPS Explorer (Applied Biosystems). Mascot software (Matrix Science, London, England) was used to search for peptide mass fingerprints and MS/MS data in the NCBInr database. Protein scores by Mascot search analysis that were >63 were considered significant ($P < 0.05$).[17,20]

Western Blotting Analysis

Tissue aliquots were homogenized to powder using liquid nitrogen and then were dissolved in lysis buffer [150 mmol/L NaCl, 50 mmol/L Tris-Cl, pH 8.0, 0.1% Nonidet P-40 (Caledon Laboratories Ltd., Georgetown, Ontario, Canada), 1 mmol/L phenylmethylsulfonyl fluoride, 25 μg/ml of aprotinin, and 25 μg/ml of leupeptin], vortexed, and incubated at room temperature for 2 hours. The mixture was centrifuged at 20,644 × g for 30 minutes at 4°C, and the supernatant was used as the total protein solution. The lysate concentration was assayed using the Bradford assay.

Western blotting analysis was performed as previously described.[17,20] Briefly, 100 μg of total protein was separated on a 12% SDS–polyacrylamide gel electrophoresis gel before being transferred onto a nitrocellulose membrane. After blocking with 5% milk in Tris-buffered saline/0.2% Tween 20 for 1 hour at room temperature, the membrane was incubated with rabbit antimouse stathmin-1 antibody (1:100 dilution) (Abcam) for 1 hour at room temperature, followed by incubation with horseradish peroxidase–conjugated goat antirabbit IgG secondary antibody (1:10,000 dilution; Amersham Biosciences) for 1 hour at room temperature. Detection of NADPH was used as a loading control. Reactions were visualized using an enhanced chemiluminescence detection system (ECL; Amersham Biosciences). Signals on the blots were visualized using autography.

Multivision IHC of Placental Tissue in Murine Models

Placentas together with decidua basalis harvested on day E10.5 from CBA/J×DBA/2J and CBA/J×BALB/c matings (none of which were analyzed by means of 2-DE) were used to measure the distribution of stathmin-1 protein in lectin from Dolichos biflorus agglutinin–positive (DBA-lectin$^+$) cells using a multivision IHC procedure. Paraffin-embedded tissue blocks were cut into 4-μm-thick sections, which were then deparaffinized in xylene and rehydrated in graded alcohol concentrations. Nonspecific binding was further blocked by preincubation with blocking solution for 5 minutes, followed by incubation for 1 hour at 4°C with rabbit antimouse stathmin-1 (1:200 dilution) (Cell Signaling Technology Inc., Beverly, MA). Meanwhile, FITC-conjugated DBA-lectin (1:200 dilution) (Sigma-Aldrich) was added onto the section in the dark for 1 hour. The sections were then washed three times with PBS for 5 minutes each and incubated with PE-conjugated antirabbit IgG (1:200 dilution) (Alpha Diagnostic International, San Antonio, TX) for 30 minutes at room temperature in the dark. Then, 4′,6-diamidino-2-phenylindole (Invitrogen, San Diego, CA) was used to stain nuclei for 10 minutes in the dark. Negative controls were established using rabbit Ig of the isotype identical to the rabbit antimouse primary antibody in place of the specific primary antibody (Cell Signaling Technology Inc.).[21]

Multivision IHC of Human Decidual Tissue

First-trimester human decidual tissue was obtained from five normal pregnancies (free of spontaneous abortion history; mean ± SD age, 27.5 ± 2.2 years; mean ± SD gestational age at sampling, 8.2 ± 1.1 weeks, terminated for nonmedical reasons) and five miscarriages [maternal history of more than three unexplained recurrent spontaneous abortions (RSAs); mean ± SD age, 32.4 ± 3.9 years; mean ± SD gestational age at sampling, 8.5 ± 2.8 weeks], which were classified as unexplained after the exclusion of maternal anatomical or hormonal abnormalities and paternal or maternal chromosomal abnormalities. All the samples were obtained from Renji Hospital, Shanghai Jiaotong University, with written informed consent from the patients and permission from the research ethics committee of Shanghai Jiaotong University.

To confirm the existence and define the distribution pattern of CD56$^+$stathmin-1$^-$ and CD56$^+$stathmin-1$^+$ cells in human decidual tissue, paraffin sections were stained with rabbit antihuman stathmin-1 (Abcam) and mouse antihuman CD56 (Lab Vision/NeoMarkers, Fremont, CA) monoclonal antibodies, followed by staining with multivision antirabbit/horseradish peroxidase (horseradish peroxidase/diaminobenzidine) plus antimouse/alkaline phosphatase polymers (Biolab Science, Beijing, China), according to the manufacturers' instructions. Using this multivision polymer detection system, stathmin-1$^+$ cells were stained brown, CD56$^+$ cells were stained red, and double-positive cells were double colored. Nuclei were lightly stained with hematoxylin.

Inhibition of Stathmin-1 in Vivo

Inhibition of stathmin-1 was performed in CBA/J×DBA/2J, CBA/J×BALB/c, and CBA/J×CBA/J matings by i.p. injection of anti–stathmin-1 antibody (GenScript USA Inc., Piscataway, NJ) on days E4.5, E5.5, and E6.5 (20 μg in 0.2 ml of PBS) once a day. Mice injected with the same volume of rabbit IgG isotype control antibody were used as controls for each group. The percentage of embryo resorption was detected on day E12.5 by using the method described previously herein (n = 8 per group).

Statistical Analysis

Flow cytometry data were analyzed by using Quad statistics.[16] The resorption rate was compared using the χ^2 test, and the cell percentage was compared using the independent-samples t-test. Cell percentage results are presented as mean ± SD.[17,18] Significance was defined at $P < 0.05$.

Results

The Percentage of Embryo Loss Is Increased in CBA/J×DBA/2J Matings

The percentage of spontaneously resorbed embryos on day E12.5 was 22.6% (35 of 155; n = 16) in CBA/J×DBA/2J matings, 7.6% (13 of 170; n = 18) in CBA/J×BALB/c matings, and 7.2% (8 of 111; n = 12) in CBA/J×CBA/J matings. There was no significant difference between CBA/J×BALB/c and CBA/J×CBA/J matings in the percentage of embryo loss, whereas the percentage of embryo resorption in CBA/J×DBA/2J matings was significantly higher than that in CBA/J×BALB/c and CBA/J×CBA/J matings ($P < 0.01$ for both). The increased resorption rate of CBA/J×DBA/2J matings supports the hypothesis that these mice are prone to spontaneous embryo loss.

Flow Cytometric Analysis of MACS-Purified CD49b$^+$ Cells

The mean ± SD percentage of stathmin-1$^+$ cells in the CD49b$^+$ NK cell population was approximately six-fold higher in CBA/J×BALB/c matings (5.2% ± 1.5%) than in CBA/J×DBA/2J matings (0.9% ± 0.4%) ($P < 0.01$), as indicated by flow cytometry (Figure 1).

Two-color flow cytometry revealed that most CD49b$^+$ cells also expressed CD122 molecules in both matings. The mean ± SD percentage of CD122$^+$CD49b$^+$ cells in the CD49b$^+$ population was 74.9% ± 11.4% in CBA/J×DBA/2J matings, which was not significantly different from that in CBA/J×BALB/c matings (65.6% ± 8.8%).

Reduced Stathmin-1 Production in uNK Cells in CBA/J×DBA/2J Matings in 2-DE

Proteins from two sets of pooled (12 pregnant mice per group) uNK cell lysates isolated from CBA/J×DBA/2J

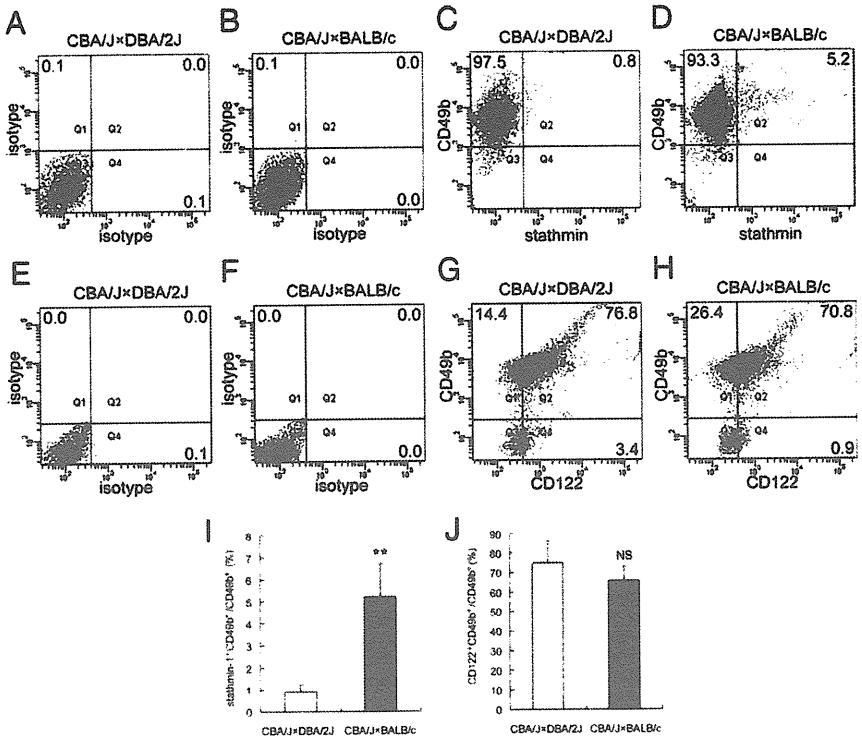

Figure 1. Flow cytometric analysis of stathmin-1$^+$ and CD122$^+$ cells in uNK cells. **A–H:** Representative results derived from cells purified using microbead-conjugated anti-CD49b and a Mini MACS. **A**, **B**, **E**, **F:** Isotype controls established using cells stained with FITC- and PE-conjugated isotype antibodies. **C**, **D:** Analysis of stathmin-1$^+$ cells in the CD49b$^+$ cell population. The cell percentage is indicated. **G**, **H:** Analysis of CD122$^+$ cells in the CD49b$^+$ cell population. **I**, **J:** Data summary of flow cytometry. Experiments were independently repeated six times in each group. The mean ± SD percentage of stathmin-1$^+$CD49b$^+$ cells was lower in CBA/J×DBA/2J mice than in CBA/J×BALB/c mice (0.9% ± 0.4% versus 5.2% ± 1.5%, $P < 0.01$). A strong CD122 signal was detected in both mating combinations. The mean ± SD percentage of CD122$^+$CD49b$^+$ cells in the CD49b$^+$ population was 74.9% ± 11.4% in CBA/J×DBA/2J mice and 65.6% ± 8.8% in CBA/J×BALB/c mice, suggesting that most of the MACS-purified CD49b$^+$ cells also express CD122. Error bars represent SD. $^{**}P < 0.01$.

matings and age-matched CBA/J×BALB/c matings on day E12.5 were resolved using 2-DE. These experiments were repeated four times under identical experimental conditions and parameters to confirm reproducibility. Well-resolved and reproducible Coomassie Brilliant Blue–stained 2-DE maps from CBA/J×DBA/2J and CBA/J×BALB/c matings were obtained. The intensity of the stathmin-1 protein spot derived from CBA/J×BALB/c matings was approximately four-fold higher than that in CBA/J×DBA/2J matings (mean ± SD, 4.1 ± 0.9-fold; $P < 0.01$) (Figure 2).

Identification and Quantification of Stathmin-1 Protein Using Matrix-Assisted Laser Desorption/Ionization–Time of Flight–MS

In the 2-DE analysis described previously herein, differentially expressed protein spots were excised from Coomassie Brilliant Blue–stained gels and were subjected to in-gel digestion with trypsin. An aliquot of the supernatant containing tryptic peptides was analyzed by means of matrix-assisted laser desorption/ionization–time of flight–time of flight–MS/MS, and the Mascot search program software package was used to identify the analyzed protein spots. Proteins receiving a significant score >63 ($P < 0.05$) in the Mascot database were ranked as the best hits. Stathmin-1 was one protein that was differentially expressed between the two sets of samples. The protein spot shown in Figure 2 was analyzed using MS and was identified as stathmin-1 (Figure 3). Stathmin-1 received a protein score of 280, a molecular weight of 17,264 Da, a pI of 5.76, and accession number gi 9789995.

The differential expression of stathmin-1 was further confirmed by immunoblots using a stathmin-1–specific antibody. The intensity of the stathmin-1 spot in CBA/J×BALB/c matings was a mean ± SD 6.9 ± 2.2–fold higher than that in CBA/J×DBA/2J matings ($^{**}P < 0.01$) (Figure 4).

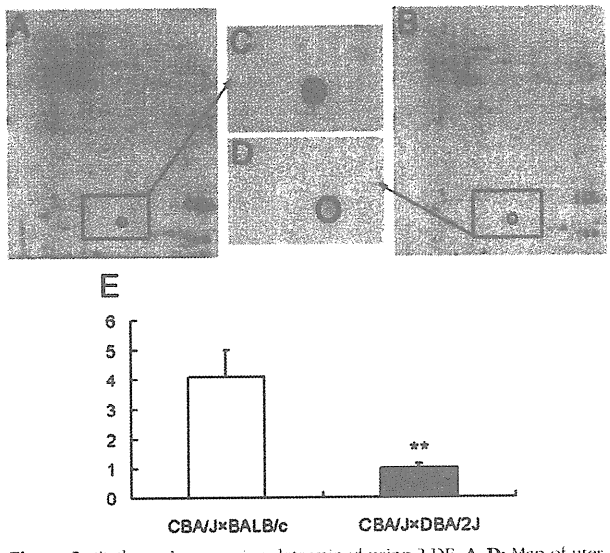

Figure 2. Stathmin-1 expression determined using 2-DE. **A–D:** Map of uterine lymphocyte lysates from CBA/J×BALB/c mice (**A** and **C**) or CBA/J×DBA/2J mice (**B** and **D**). **C** and **D** indicate the original magnification of the stathmin-1 protein spot from CBA/J×BALB/c and CBA/J×DBA/2J mice, respectively. The density of the stathmin-1 protein spot from CBA/J×BALB/c mice was higher than that from CBA/J×DBA/2J mice as observed by the naked eye. **E:** Mean density as determined using Image-Pro Plus 6.0. The mean density of stathmin-1 spots in CBA/J×BALB/c mice was a mean ± SD 4.1 ± 0.9–fold higher than that in CBA/J×DBA/2J mice ($^{**}P < 0.01$). Experiments were independently performed four times. Error bars represent SD.